AD-A066 151 PENNSYLVANIA STATE UNIV UNIVERSITY PARK IONOSPHERE R--ETC F/G 17/2.1
COMBINATION FREQUENCY AND VLF-ELF GENERATIONS THROUGH HIGH-POWE--ETC(U)
FEB 79 A J FERRARO, H S LEE N00014-77-C-0041

UNCLASSIFIED PSU-IRL-FR-79/1 NL

1 OF 1
AD A
066151

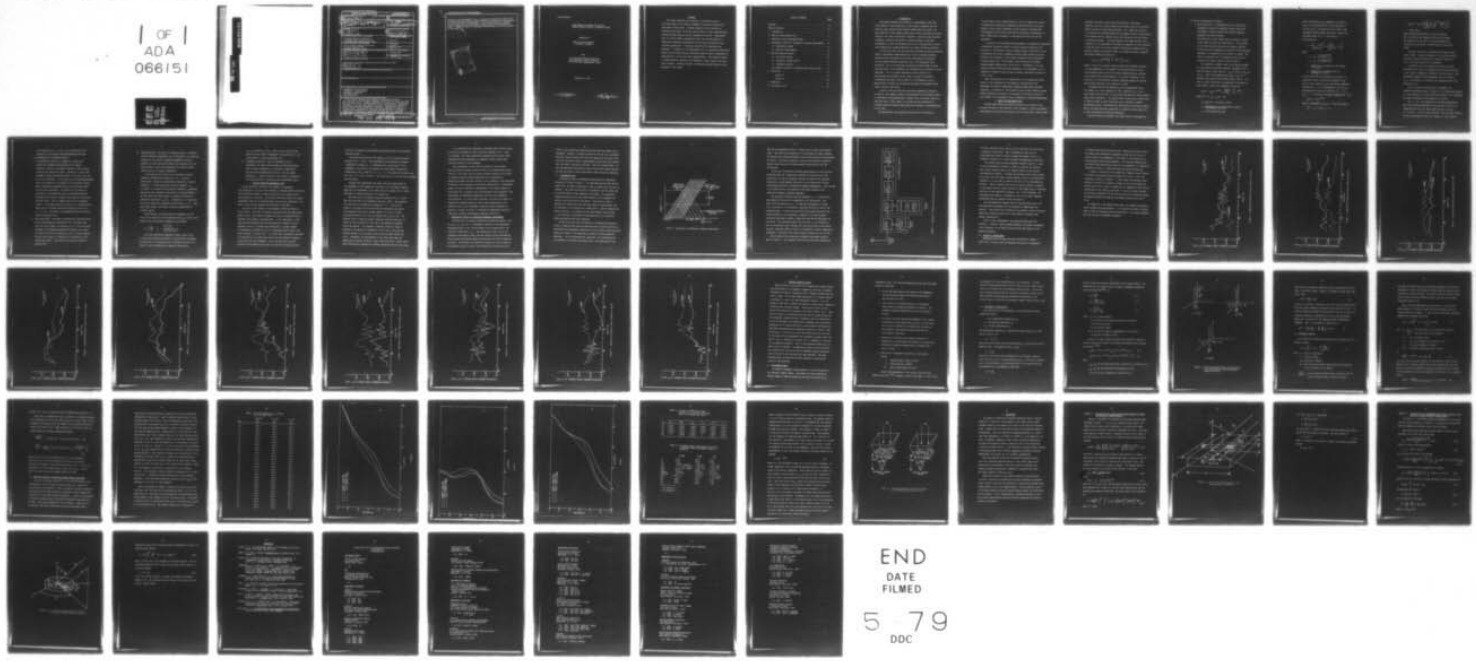

END
DATE
FILMED
5 79
DDC

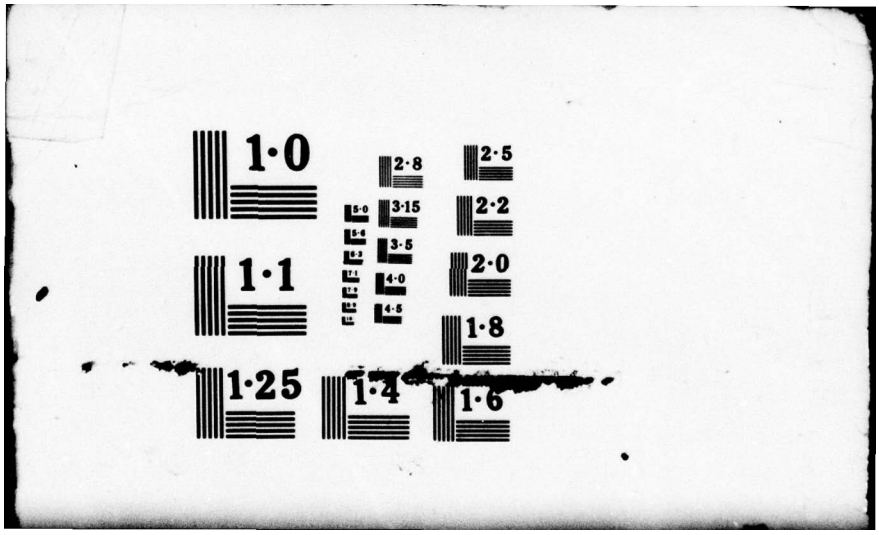
1·0
1·1
1·25
2·8
3·15
3·5
4·0
4·5
2·5
2·2
2·0
1·8
1·4
1·6

SECURITY CLASSIFICATION OF THIS PAGE (When Data Entered)

REPORT DOCUMENTATION PAGE

READ INSTRUCTIONS BEFORE COMPLETING FORM

1. REPORT NUMBER: PSU-IRL-FR-79-2	2. GOVT ACCESSION NO.
3. RECIPIENT'S CATALOG NUMBER	
4. TITLE (and Subtitle): Combination Frequency and VLF-ELF Generations Through High-Power HF Heating of D-Region Ionosphere.	5. TYPE OF REPORT & PERIOD COVERED: Final Report, 1 Nov 1976 - 31 Oct 1978
	6. PERFORMING ORG. REPORT NUMBER
7. AUTHOR(s): A. J. Ferraro, H. S. Lee	8. CONTRACT OR GRANT NUMBER(s): N0014-77-C-0041
9. PERFORMING ORGANIZATION NAME AND ADDRESS: Ionosphere Research Laboratory, The Pennsylvania State University, University Park, Pennsylvania 16802	10. PROGRAM ELEMENT, PROJECT, TASK AREA & WORK UNIT NUMBERS: NR 089-120
11. CONTROLLING OFFICE NAME AND ADDRESS: Office of Naval Research (Code 465), 800 North Quincy Street, Arlington, Virginia 22217	12. REPORT DATE: 2/21/79
	13. NUMBER OF PAGES: 52
14. MONITORING AGENCY NAME & ADDRESS (if different from Controlling Office): 21 Feb 79	15. SECURITY CLASS. (of this report): Unclassified
	15a. DECLASSIFICATION/DOWNGRADING SCHEDULE: N/A

16. DISTRIBUTION STATEMENT (of this Report)

Distribution unlimited; cleared for public release and sale.

62 p.

17. DISTRIBUTION STATEMENT (of the abstract entered in Block 20, if different from Report)

18. SUPPLEMENTARY NOTES

19. KEY WORDS (Continue on reverse side if necessary and identify by block number)

Ionospheric Non-Linearities;
Ionospheric Current System;
Ionospheric Radiation;
Cross Modulation.

20. ABSTRACT (Continue on reverse side if necessary and identify by block number)

This report describes the outcome of a preliminary study of non-linearities in the D-region ionosphere by heating the region with high power HF radio waves. Ultimate objective of the study was in determining the impact of the non-linear effects on radio communications, especially under highly disturbed ionospheric conditions. Experimental work of "Initial Phase" investigation dealt with the measurement of combination frequencies generated by the high power heating wave and a low power probing wave. Preliminary results of the measurement are presented. In

DD FORM 1 JAN 73 1473 EDITION OF 1 NOV 65 IS OBSOLETE
S/N 0102-014-6601

188 150

SECURITY CLASSIFICATION OF THIS PAGE (When Data Entered)

addition to the experimental work, a theoretical feasibility study of the so-called wireless radiation system was made to determine its applicability to ELF and ULF radio communications. This radiation system is brought about by modulating the ionospheric current system using high-power HF heater. Numerical results of predicted radiated powers are also presented in this report.

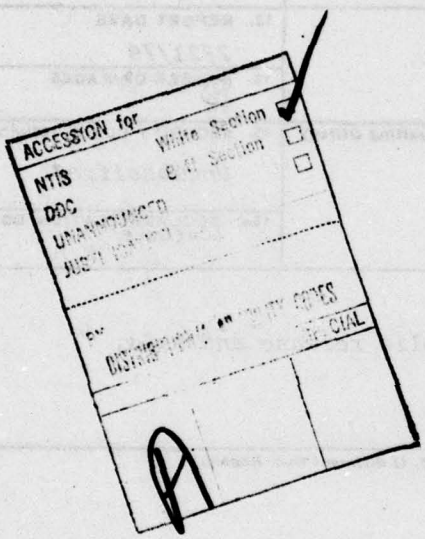

PSU-IRL-FR-79/1

Final Report and Summary of D-Region Research Under Grant No. N00014-77-C-0041.

Submitted to

Office of Naval Research
Arlington, Virginia

From

The Ionosphere Research Laboratory
The Pennsylvania State University
University Park, Pennsylvania 16802

February 21, 1979

A. J. Ferraro

H. S. Lee

Abstract

This report describes the outcome of a preliminary study of non-linearities in the D-region ionosphere by heating the region with high power HF radio waves. Ultimate objective of the study was in determining the impact of the non-linear effects on radio communications, especially under highly disturbed ionospheric conditions. Experimental work of "Initial Phase" investigation dealt with the measurement of combination frequencies generated by the high power heating wave and a low power probing wave. Preliminary results of the measurement are presented. In addition to the experimental work, a theoretical feasibility study of the so-called wireless radiation system was made to determine its applicability to ELF and ULF radio communications. This radiation system is brought about by modulating the ionospheric current system using high-power HF heater. Numerical results of predicted radiated powers are also presented in this report.

TABLE OF CONTENTS

1. INTRODUCTION

This report describes the outcome of an experimental study made, on the effects of non-linearities in the D-region ionosphere, for the Office of Naval Research under Contract Number N00014-77-C-0041. The main objective of this research effort was to better understand non-linear effects in the normal and abnormal ionosphere, especially under anomalous ionospheric conditions due either to natural phenomena or man-made disturbances, so that the knowledge could aid in developing more reliable radio communication systems appropriate for highly disturbed ionosphere.

In view of the fact that the non-linear phenomena are weak second-order effects, experimental measurements had to rely on extremely sensitive detecting device developed for the radio cross-modulation experiment at the Ionosphere Research Laboratory (IRL), The Pennsylvania State University. As for the high-power transmitting system needed to create non-linearities in the ionosphere, two transmitters were available for this experiment. One is a pulsed transmitter normally used for the cross-modulation experiment at IRL, which is capable of radiating 15 Megawatts peak power, and the other is a CW transmitter, with 10 Megawatts ERP, available at the National Astronomy and Ionosphere Center (NAIC), Arecibo, Puerto Rico.

In spite of the fact that such non-linear phenomena are difficult to observe, this research endeavor was encouraged by the favorable reports of experimental measurements made in Russia, Italy and France, which are described later in this report, on one hand and the availability of extremely sensitive sophisticated digitalized detector of cross-modulation on the other.

The experimental work reported here deals with the outcome of

"Initial Phase" of the research program in which an emphasis was placed on observing the combination frequencies resulting from the non-linear effects in the D-region ionosphere; mainly relying on existing radio cross-modulation facilities at IRL and the high-power CW transmitter at NAIC, without major investments in developing new facilities for the experiment.

In parallel to this experimental measurements of combination frequencies, a theoretical feasibility study of wireless radiating system was also carried out. The concept of such a radiating system is based on the idea of modulating the natural ionospheric current system through controlled heating of the electrons in the D-region ionosphere using a high-power HF pulsed radio waves. This concept is very suitable for extremely long-wavelength communications at ELF or ULF. Furthermore, it is very closely related with the non-linear phenomena in the ionosphere as it is discussed in connection with the work of Russian scientists, in Section 3 of this report.

Since the objective of our research work is in studying non-linear effects in the ionosphere for the purpose of contributing to the development of workable communication systems through highly disturbed ionosphere, the theoretical investigation of the wireless radiating system seemed important and relevant to be included in this report along with the findings of the experimental work of combination frequency measurements.

2. BASIS FOR EXPERIMENTAL WORK

The non-linear effects are basically caused by two factors: first, the mean free path of the electrons in the ionosphere is quite considerable, and therefore the electrons may acquire from the radio waves a large energy;

secondly, the energy transfer from the electrons to the atoms, molecules, and ions is made difficult by the small ratio of the electron mass to the mass of these heavy particles. As a result the electrons in an electric field become heated and the complex dielectric permittivity of the medium begins to depend on the field intensity, and thus acquire a non-linear character. The significance of non-linear effects in the ionosphere can be approximately evaluated by comparing the field intensity of the radio wave E with the so-called "characteristic plasma field" E_p given by Ginzburg and Gurevich (1960) for a simple isotropic ionosphere. The effects become significant for

$$E \gtrsim E_p = \sqrt{3\ k\ T\ \frac{m}{e^2}\ G\ (\omega^2 + \nu_o^2)}\ \ [v/m]$$

where e, m and k are electron charge and mass and Boltzmann's constant, T is the temperature in the absence of the applied electric field, G is the average relative fraction of energy transferred upon collision of an electron with a heavy particle, ω is angular frequency of the field and ν_o is the effective collision frequency between the electron and the heavy particles in the absence of a field.

Estimates show that the quantity E_p is not unreasonably large. For example, for a wave frequency of 5 MHz, typically $E_p \lesssim 1$ v/m in the D-region; with the value of E_p getting even smaller at higher heights and/or lower frequencies. This implies that the non-linear effects could be created without too much difficulty with a reasonably powerful transmitting system. Nevertheless the observations of non-linear effects made in the past have been a qualified or a limited success largely due to lack of sophisticated detecting techniques.

The most important ionospheric non-linear effects investigated up

to now can be summarized as follows:

a) Self-interaction: As mentioned earlier, a strong wave propagating through the ionospheric medium could alter the complex dielectric permittivity through thermally dependent collisional process.

The strong wave, which created such non-linearity, itself is not immune from the non-linear effects. This results in the self-interaction wherein the frequency spectrum of the strong wave (appearance of harmonics of the principal frequency), its absorption and its phase all change. The effect on absorption will be discussed briefly below to illustrate the general feature of non-linearity.

For simplicity, assume a wave to be normally incident on a horizontally stratified isotropic ionosphere at $z = 0$ with the electric field given by: $E_{10}(z) \cos \omega_1 t = E_{10}(0) \cos \omega_1 t$. Under the assumption that $E_{10}(0) \gtrsim E_p$, the characteristic plasma field defined earlier, and $\omega >> G\nu$, which is usually satisfied, the amplitude of the wave at a given height z within the ionosphere is given by:

$$E_{10}(z) = E_{10}(0)\, e^{-K(z)}\; p\left[\frac{E_{10}(0)}{E_p}\,,\ \frac{\omega_1}{\nu_o}\,,\ K(z)\right]$$

where $k(z) = k_o \int_o^z \chi_o(z')\, dz'$

$k_o = \frac{\omega_1}{c}$ with c = velocity of light

χ_o = imaginary part of the refractive index in the absence of the wave

p = self-interaction factor

Since the amplitude $E_{10}(z)$ depends on the factor p and p in turn depends on the initial magnitude of the wave $E_{10}(0)$, the absorption of the wave in the ionospheric medium becomes non-linear. Deep in the ionosphere where $K(z) > > 1$, the factor p can be given by:

$$p = 2 \frac{E_p}{E_{10}(0)} \left(\frac{\tau_o - 1}{\tau_o + 1} \right)^{\frac{1}{2}} \exp \left[\frac{2\nu_o^2}{\omega_1^2 + \nu_o^2} (\tau_o - 1) \right]$$

where

$$\tau_o = \tau(0) = \left(\frac{T_e [E_{10}(0)]}{T} \right)^{\frac{1}{2}}$$

$$\tau = \tau(z) = \left(\frac{T_e [E_{10}(z)]}{T} \right)^{\frac{1}{2}}$$

T = Temperature of electrons in the absence of the wave

T_e = Temperature of electrons which is dependent on E field

As can be seen from the expression the factor p is explicitly as well as implicitly dependent on the initial field intensity $E_{10}(0)$ and through temperature related term τ_o. It is interesting to note that for high-frequency strong waves such that $\omega_1^2 > > \nu_o^2 \tau_o$ and $\tau_o > > 1$, the factor p becomes independent of τ_o and

$$E_{10}(z) = 2 E_p E^{-K(z)}$$

which is independent of $E_{10}(0)$. On the other hand if

$$\omega_1^2 < < \nu_o^2 \tau_o \text{ and } \tau_o > > 1,$$

$$E_{10}(z) = 2\,E_p \exp\left[2\left\{\left(\frac{\nu_o^2}{\omega_1^2+\nu_o^2}\right)^{3/2}\frac{E_{10}(0)}{E_p}\right\}^{\frac{1}{2}}\right]$$

$$\cdot \exp\,[-K(z)]$$

which increases exponentially as $E_{10}(0)$ increases. Thus for the very low frequency, deep into the plasma, the absorption of the wave is very much reduced for a strong wave as the result of self-interaction non-linear effect.

In general the factor p approaches unity when the wave field is weak. The above discussion is for electron-molecule collision dominant case which is a reasonable assumption for D- and lower E-region of the ionosphere.

In addition to the non-linear self-interaction effect described above, there is a secondary time-varying perturbation in the electron temperature inflicted by the strong wave. This perturbation appears in the frequencies that are multiples of ω_1. This behavior is related to the frequency mixing to be described in (d).

Up to this point the strong wave was assumed to be unmodulated continuous waves. However, if it is amplitude-modulated at a low frequency Ω, the self-interaction effect in the ionosphere may change substantially the modulation of the wave.

For $\Omega << G\nu_o$, the propagation of the amplitude-modulated wave can be treated essentially in the same way as that of an unmodulated wave was, by simply replacing $E_{10}(0)$ by $E_{10}(0)$ $\cdot(1 + M \cos \Omega t)$. In such a case, because of the non-linear effects, not only the modulation index M is changed but also harmonics

with frequencies 2 Ω, 3 Ω, etc., are introduced with the alteration in the shape of amplitude-modulated envelope.

b) Cross-modulation (Luxembourg Effect):

As evidenced in section (a), passage of a strong wave through the ionospheric medium perturbs the complex dielectric constant of the medium resulting in non-linearity affecting the strong wave itself. Obviously, if other waves propagate through the perturbed region, at the same time, they will also be affected. If the strong wave is amplitude-modulated with a low frequency Ω, the medium will be perturbed likewise. When a second wave propagates through this perturbed medium, it will also he modulated. This effect can be viewed as a transferral of the modulation from one amplitude-modulated high-power radio signal to another while they are transversing the same region. This is commonly known as the "Luxembourg Effect." As discussed earlier in section (a), cross-modulation takes place at principal modulation frequency as well as at 2 Ω, 3 Ω, etc. The effect of cross-modulation has been widely used as a diagnostic tool.

c) Gyro-interaction: The effect is essentially a modified version of the cross-modulation described in (b) in the sense that while the basic concept is the same as in (b), here the carrier frequency of the amplitude-modulated high-power radio signal was chosen near the gyro-frequency in order to greatly magnify the non-linear effect in transferring the modulation to the second radio signal. This effect was initially studied by Bailey (1937).

d) *Frequency Mixing:* The effect of frequency mixing, or sometimes called combination frequencies, can be discussed in two different categories. One is due to thermally dependent collisional process as all the non-linear effects were discussed up to now and the other is due to the perturbation in electron density rather than that in electron temperature.

The former has its origin in the time-varying electron temperature perturbation pointed out in (a). Since this perturbation, created by an unmodulated strong wave of angular frequency ω_1, is time-varying with angular frequency $2\omega_1$, or higher, if a second wave with angular frequency ω_2 propagates through the same ionospheric region which is being perturbed, it has been shown that they interact to produce the waves with combination frequencies $\omega_2 \pm 2\omega_1$. Furthermore, it is found that the mixing effect has a resonance condition when $\omega_2 = 2\omega_1$. Also, among other things, this effect is directly proportional to electron density.

These behaviors are obvious from the expression for the ratio of the amplitude of the combination wave E_{21} to that of the second wave E_2 with angular frequency ω_2 given below:

$$\eta = \left| \frac{E_{21}}{E_2} \right| \sim \frac{e^4 E_1^{\,2} N\nu_o}{m^2 \omega_1^{\,3} kT(\omega_2 - 2\omega_1)^2}$$

The second combination-frequencies effect, which is due to the electron density perturbation resulting from the passage of strong wave, is characteristically different from the first effect in that the combination frequencies produced are

$\omega_1 \pm \omega_2$ instead of $\omega_2 \pm 2\omega_1$. This is due to the fact that while the first effect is dependent on the quantity E_1^2, the second effect is linearly dependent on E_1.

e) Ionospheric Detection: This is considered to be an ionospheric non-linear effect whereby the modulating signal with an angular frequency ω_s is detected or demodulated from the amplitude-modulated wave with a carrier angular frequency ω_c. Physical details of this effect is presented in the following section "Relevant Previous Experimental Work."

3. RELEVANT PREVIOUS EXPERIMENTAL WORK

As the scientific interest in the subject of ionospheric non-linearities is as old as the discovery of Luxembourg Effect there have been considerable amount of research work done in the general area of non-linearities in the past. Only several relatively recent and relevant experimental work will be described here since they are considered to be more in line with the interest and objectives of this work.

The first is the concept of the ionospheric detection effect by Cutolo (1964). This work is extremely interesting from the applications point of view. This effect as reported by Cutolo is characteristically different from standard cross-modulation. In his experiments, a high power VHF wave modulated with the gyro-frequency, instead of a gyro-frequency carrier in classical gyro-interaction, is beamed towards the ionosphere coincident with an H.F. unmodulated wanted signal; both waves intersect at around 90 km. It is found that considerable modulation is transferred to the second wave only if the VHF modulation frequency is near the local gyro-frequency. It was concluded that the gyro-modulation was demodulated and acted as a gyro-wave disturbing signal

just as in an ordinary cross-modulation experiment using a gyro-frequency disturbing signal.

The second related work on the subject is that of French scientists Lavergnat et al., (1977). This experimental work successfully observed a combination frequency $f_1 - \Delta f$ generated near f_2 peak region of the ionosphere as the result of two powerful UHF radio waves transmitted at frequencies f_1 and f_2 where $\Delta f = f_2 - f_1$. f_1 = 934.25 MHz and Δf=2MHz in one case and Δf = 5.1 MHz in another. Each radio wave had 75 KW fed into an antenna with 50 db gain.

Although this experimental work dealt with much higher region of the ionosphere at UHF frequencies, the report of its successful measurements was an encouragement to our effort which was aiming to do a similar experiment at D-region altitude at HF frequencies.

The third work is by Russian scientists Getmantsev et al., (1974). This work also deals with ionospheric detection effect. They observed the radio wave at the modulation frequency of 1.2 $\sim$ 7 KHz on the ground at a distance of 180 Km away from the high-power transmitter. The transmitter delivered an average power of 130 Kw at 5.75 MHz, amplitude-modulated at 95%, into an antenna with a gain of 150. The Russians used an elaborate coherent detection system and were able to measure a field intensity of 0.02μ v/m at the modulation frequency during the daytime. The ionospheric detection effect was found to maximize at the modulation frequency of 2.5 KHz and at noon when the electron density is at its peak and the effect was absent during the night. Furthermore, the measurements of the signal made under the magnetically disturbed conditions, while they varied over a larger range, quite often greatly exceeded the intensity observed during the quiet days.

It is interesting and important to note that some of the co-authors of this work concluded, in their later work (Mityakov et al. - 1976), in retrospect, that their observations presented here are most likely associated with the modulation of ionospheric current system under artificial heating of the ionosphere.

Such a phenomenon is also directly related to the so-called wireless radiating system suitable for ELF or ULF communication system. Authors of this report have had strong interest recently on the subject of wireless radiating system; especially on the feasibility of modulating D-region and lower E-region of the ionosphere, using high-power HF heating, for the purpose of ELF and ULF communications. Considerable amount of initial theoretical investigation of the subject matter has been carried out in parallel with the experimental work performed on the measurements of combination frequencies resulting from ionospheric non-linearities. In view of their relevancy, in terms of our effort in searching for possible means for future radio communications, the theoretical work on the ionospheric modulation using high-power HF heating is included in Section 5 following the experimental results of combination frequency measurements presented in Section 4.

4. EXPERIMENTAL RESULTS OF COMBINATION-FREQUENCY MEASUREMENTS

Although there are numerous combination frequencies possible, such as $\omega_2 \pm \omega_1$, $\omega_2 \pm 2\omega_1$, etc., as discussed in Section 2, the experimental measurements made in this "Initial Phase" of our research effort was limited to observing $\omega_2 - 2\omega_1$. This observation relies only on the temperature perturbation rather than the electron density perturbation which requires considerably higher heating power than that is presently available. Furthermore, the difference frequency was tried instead of sum frequency, again in view of the availability of the facilities in

order to avoid additional budget which would have been needed for new equipments. However, it should be noted that the new NAIC high-power facilities which are being built and to be operational by August, 1979, will have 200 MW ERP, which is approximately twenty times more powerful than the present high-power facilities. With the increased power, not only the temperature perturbation effect will be more readily observed, but also the electron density perturbation effect should be observable.

4.1 EXPERIMENTAL DATA

The general scheme of experimental observations of combination frequencies is shown in Figure 1. The high-power heating wave and the second wave, of angular frequencies ω_1 and ω_2 respectively, are sent up together. The former is much wider in pulsewidth than the latter and is initiated ahead in time compared to the latter. Any combination frequency generated due to non-linear effects in the ionosphere will return to and be observed on the ground. Time gating is used to determine the height where the non-linear effect is taking place, and the pulsewidth of the second wave is made short in order to enhance the height resolution. By varying the time delay between the two waves, τ_D, any variation in the effect of non-linearities as a function of height and heating time can be observed.

In view of the fact that the detection of combination frequencies relied on sophisticated sensitive detecting device already available for cross-modulation experiments conducted at IRL the general scheme described above had to adapt to the operational procedures of cross-modulation experiment. In the cross-modulation experiment, the disturbing pulse is transmitted at one-half the pulsing rate of the probing pulse such

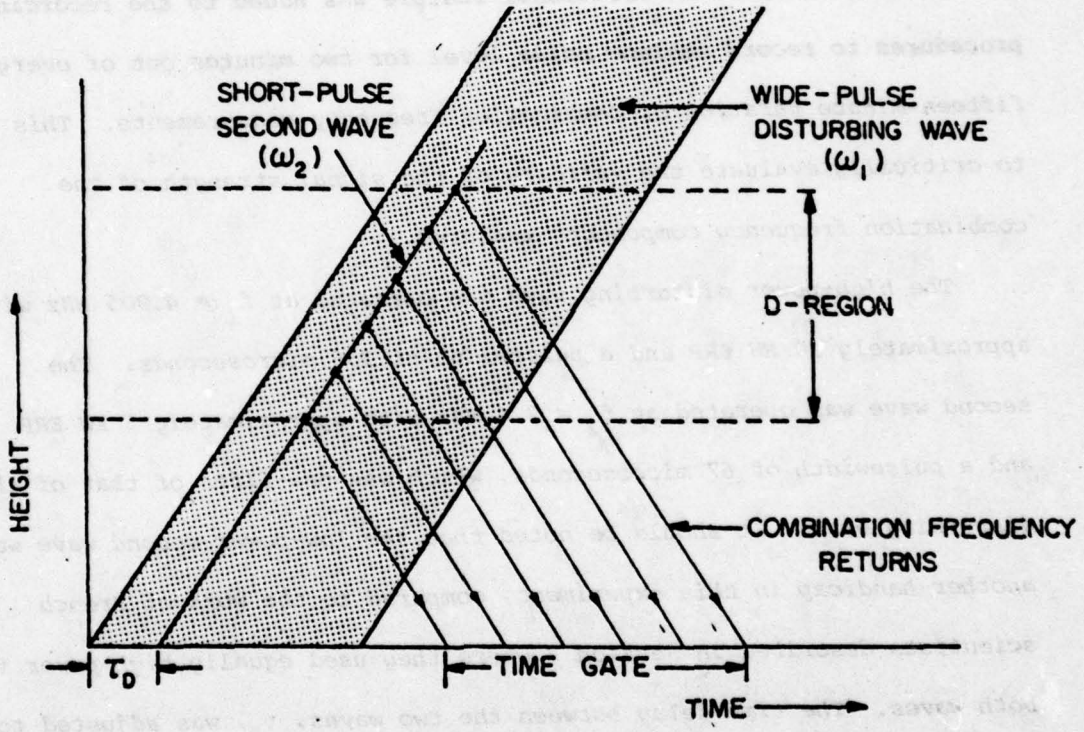

FIGURE 1: Description of Combination Frequency Measurement.

that the cross-modulation effect is taking place on every other probing pulse. This makes the determination of cross-modulation effect possible by detecting the difference between the two probing pulses with and without the effect. The slight difference is detected and digitally recorded on magnetic tape covering 28 D-region heights simultaneously every 300 milliseconds.

In the case of combination frequency measurements not only the wide disturbing pulse was transmitted at one-half the pulsing rate of the second wave, but also an additional feature was added to the recording procedures to record ambient noise level for two minutes out of every fifteen-minute duration of combination frequency measurements. This was done to critically evaluate the validity of the signal strength of the combination frequency components measured.

The high-power disturbing wave was operated at f_1 = 4.905 MHz with approximately 10 MW ERP and a pulsewidth of 335 microseconds. The second wave was operated at f_2 = 2.4 MHz with approximately 5 KW ERP and a pulsewidth of 67 microseconds, which was one-fifth of that of the disturbing wave. It should be noted that the low-power second wave was another handicap in this experiment, compared to the work of French scientists described in Section 3 where they used equally high-power for both waves. The time delay between the two waves, τ_D, was adjusted to have the second-wave pulse coincide with the trailing end of the disturbing wave. Time gate shown in Figure 1 was adjusted to monitor combination frequencies originating from D-region heights ranging from 54 to 90 Km.

Block diagram for the combination frequency measurement system is shown in Figure 2. The converter block receives difference frequency of

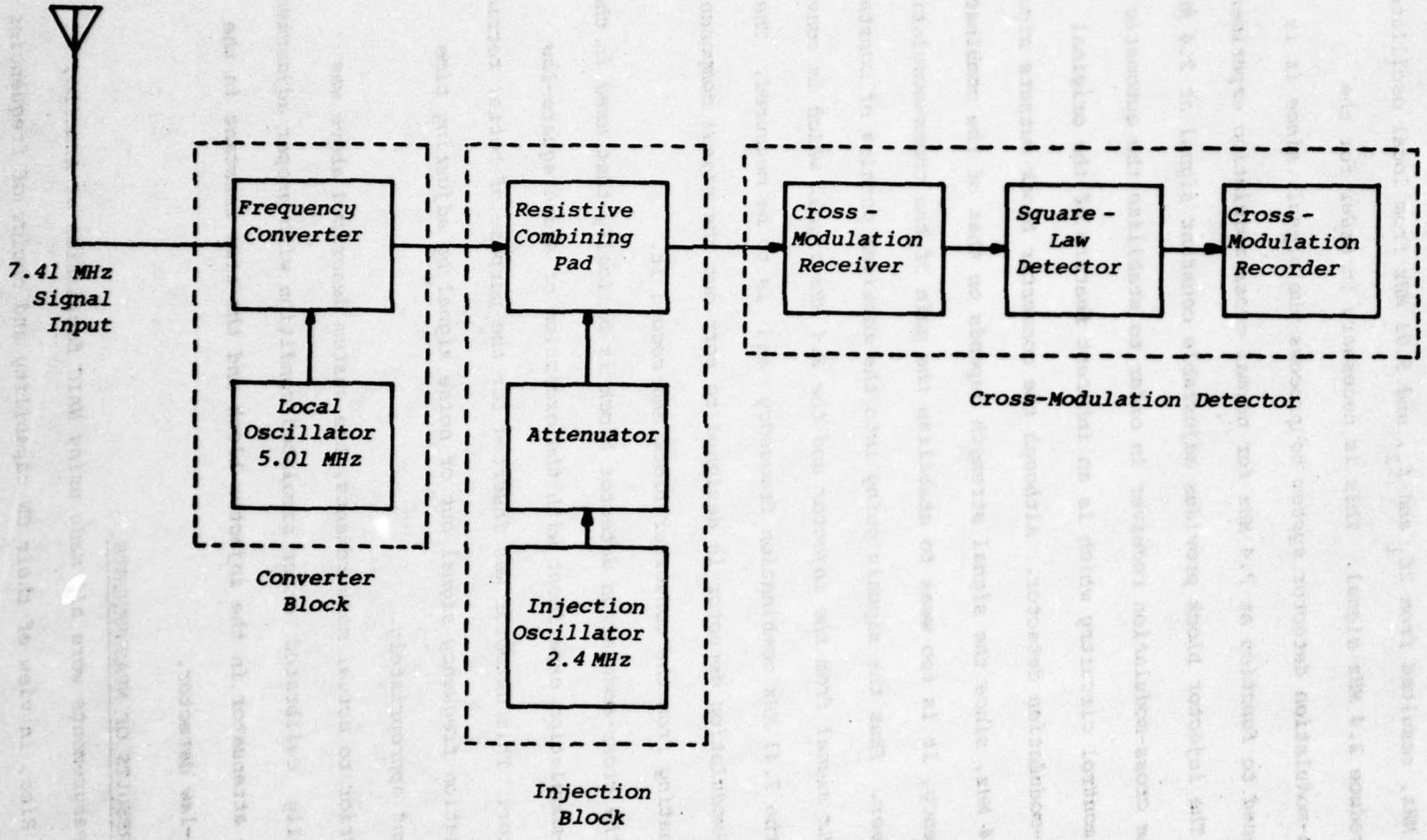

FIGURE 2: Combination Frequency Detecting System Block Diagram.

7.41 MHz, resulted from $2f_1$ and f_2, and 5.01 MHz from local oscillator to produce 2.4 MHz signal. This is necessary in order for the cross-modulation detector system to process the signal, since it is designed to function at 2.4 MHz for normal cross-modulation experiment.

The injector block provides adjustable constant signal at 2.4 MHz to the cross-modulation receiver in order to stabilize the automatic gain control circuitry which is an inherent feature of the original cross-modulation detector. Although the converter block outputs signals at 2.4 MHz, since the signal strength depends on that of the combination frequency, it is too weak to stabilize the gain of the cross-modulation receiver. Thus the signals going into the receiver consist of constant 2.4 MHz signal from the injector and the 2.4 MHz signal which is converted from the 7.41 MHz combination frequency and is to be measured. The cross-modulation detector is designed to sort out the signal component originating from the converter block and record it.

The cross-modulation detector block is basically that used in the cross-modulation experiment with the exception of added square-law detector. This detector was inserted for the purpose of better retrieving combination frequency signal out of noise signal by adjusting time constant appropriately.

Prior to actual measurements, the system described above was carefully calibrated under simulated condition with proper adjustments of the attenuator in the injector block and the time constant in the square-law detector.

4.2 RESULTS OF MEASUREMENTS

Measurements were all made using NAIC facilities at Arecibo, Puerto Rico, in view of their CW capability and choice of frequencies

in radiating high-power disturbing waves. Whenever possible an effort was made to make measurements throughout varying time of the day in order to observe the dependency of the effects of non-linearities on electron density among other parameters. This was done because while the effect being observed was related to the perturbation of temperature, according to theory, it linearly depended upon electron densities.

A typical illustration of the combination frequency signal observed from 0930 in the morning through noontime AST on June 21, 1977, are presented in Figures 3 through 12. On each figure the observed signal strength is plotted as a function of height in solid line whereas the ambient noise level is given in dashed line for comparison. Time interval represented by each figure is also given. One unit of signal strength in the figure represents 10^{-8} volts at the input of the detecting system. The signal strengths are shown for the heights ranging from 54 km to 90 km.

In comparison to the ambient noise level, the combination frequency signal strength does seem marginal. It is believed to be due to limited power in both the disturbing and the second waves. The results presented here will further be discussed in Section 6.

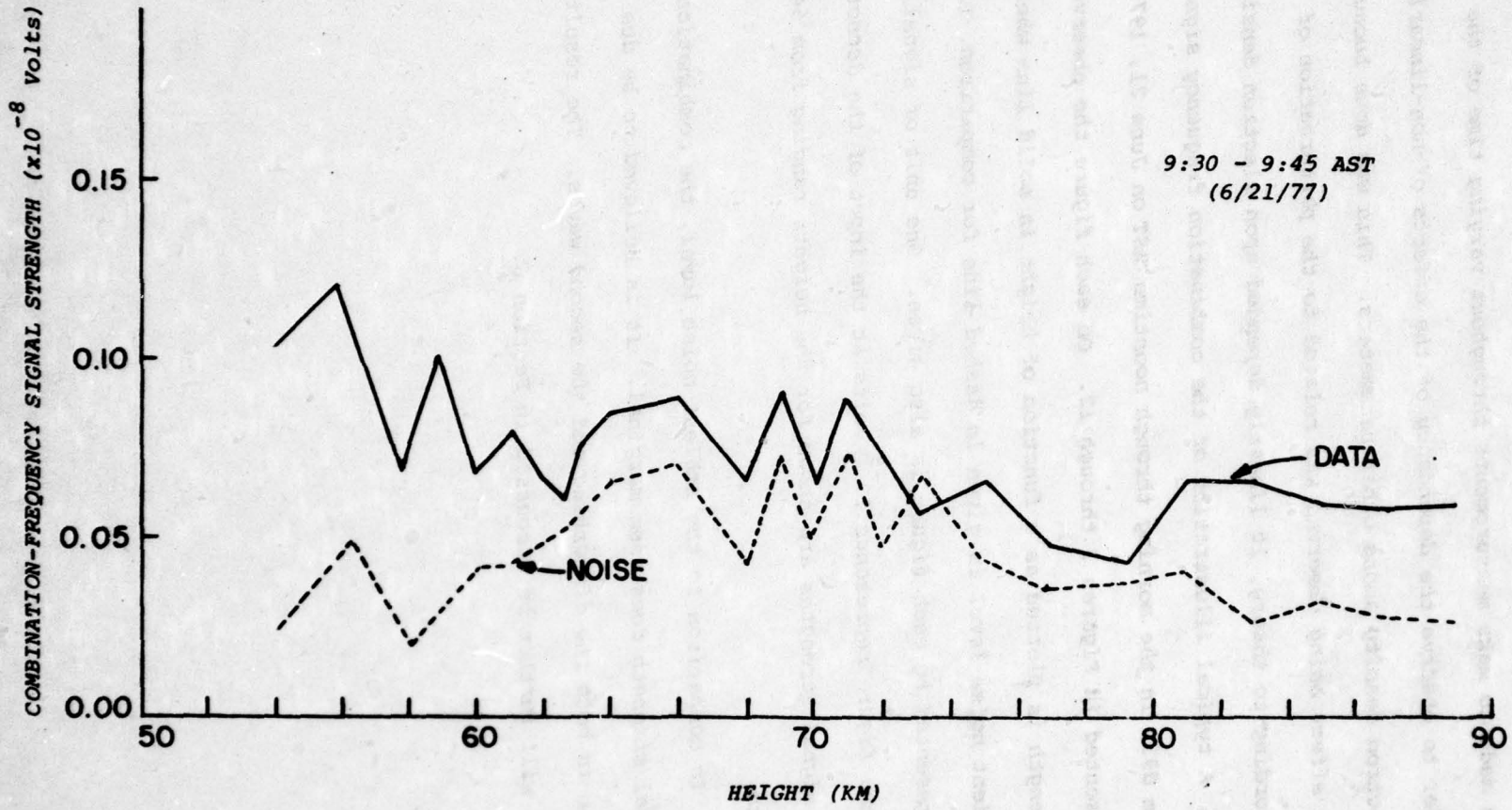

FIGURE 3: Combination-Frequency Signal Strength vs Height.

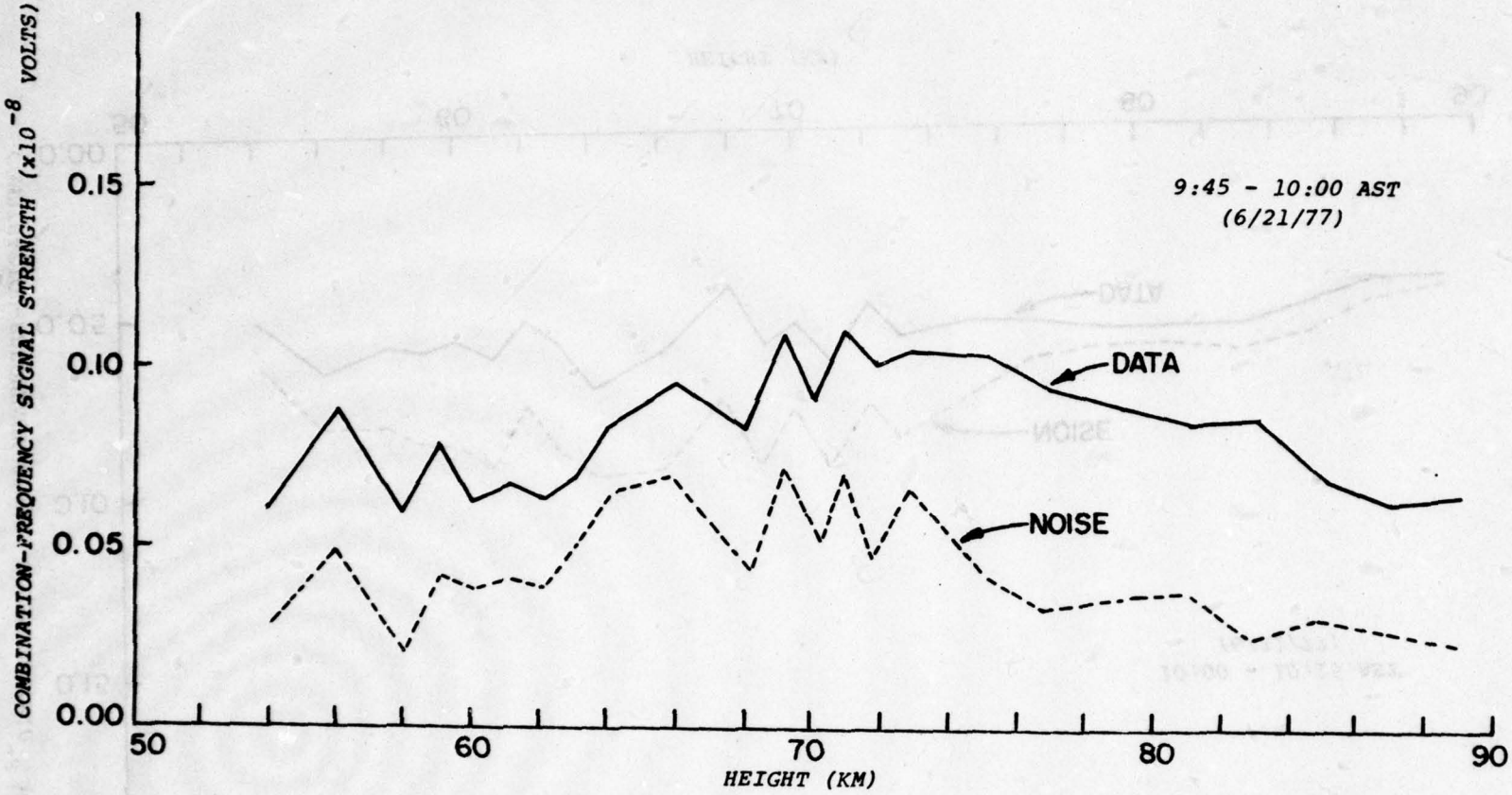

FIGURE 4: Combination-Frequency Signal Strength vs Height.

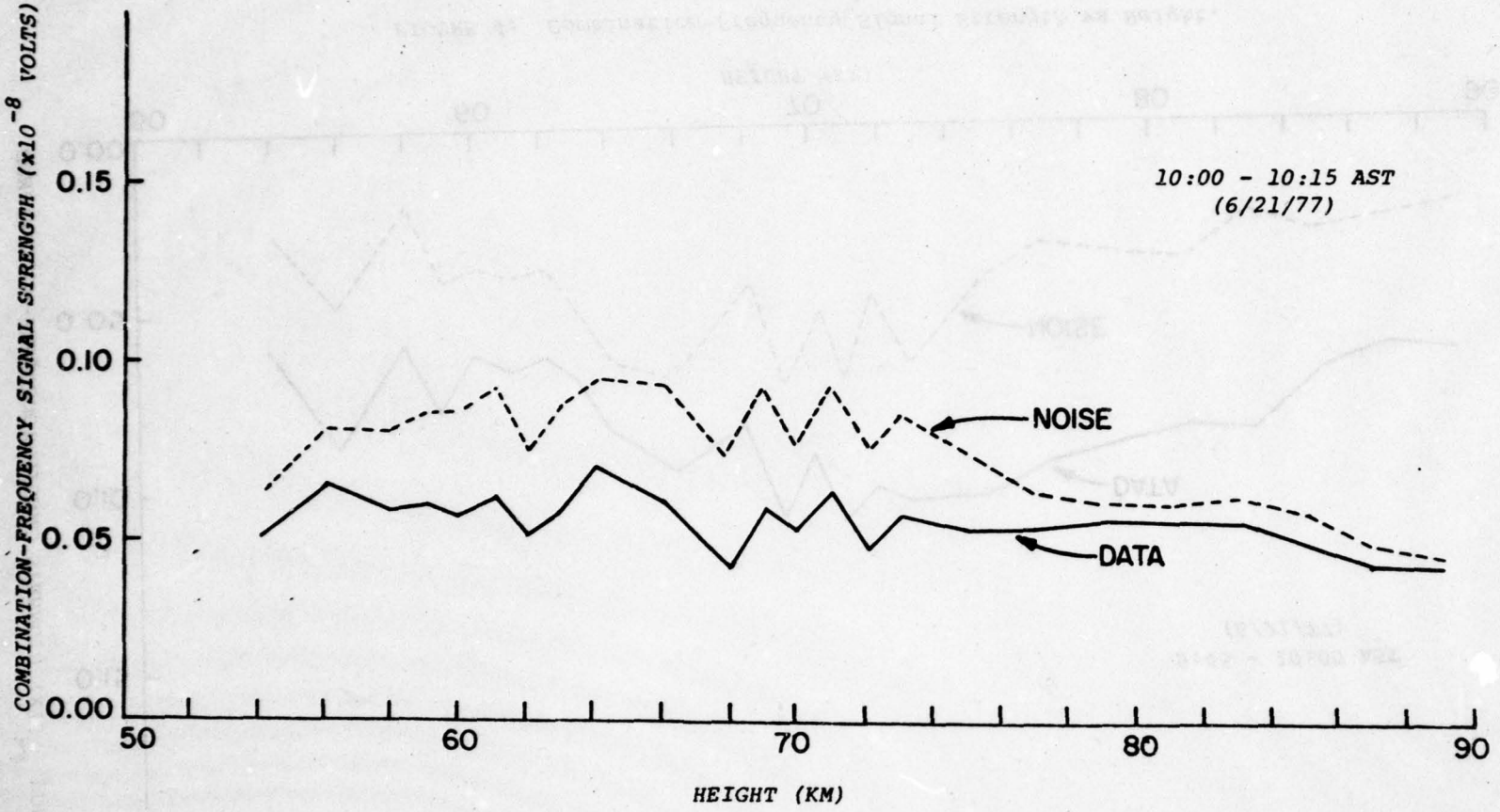

FIGURE 5: Combination Frequency Signal Strength vs Height.

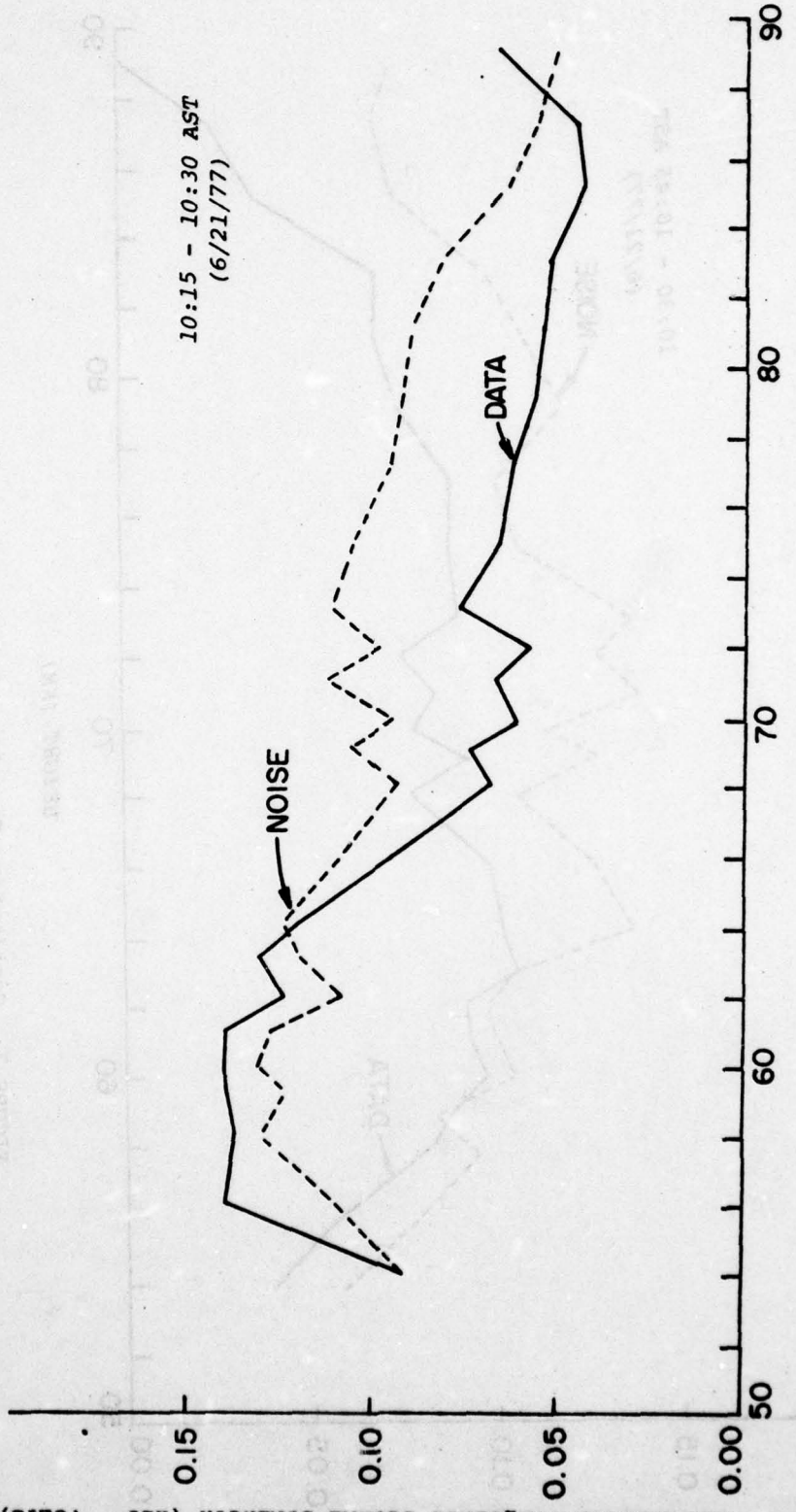

FIGURE 6: Combination-Frequency Signal Strength vs Height.

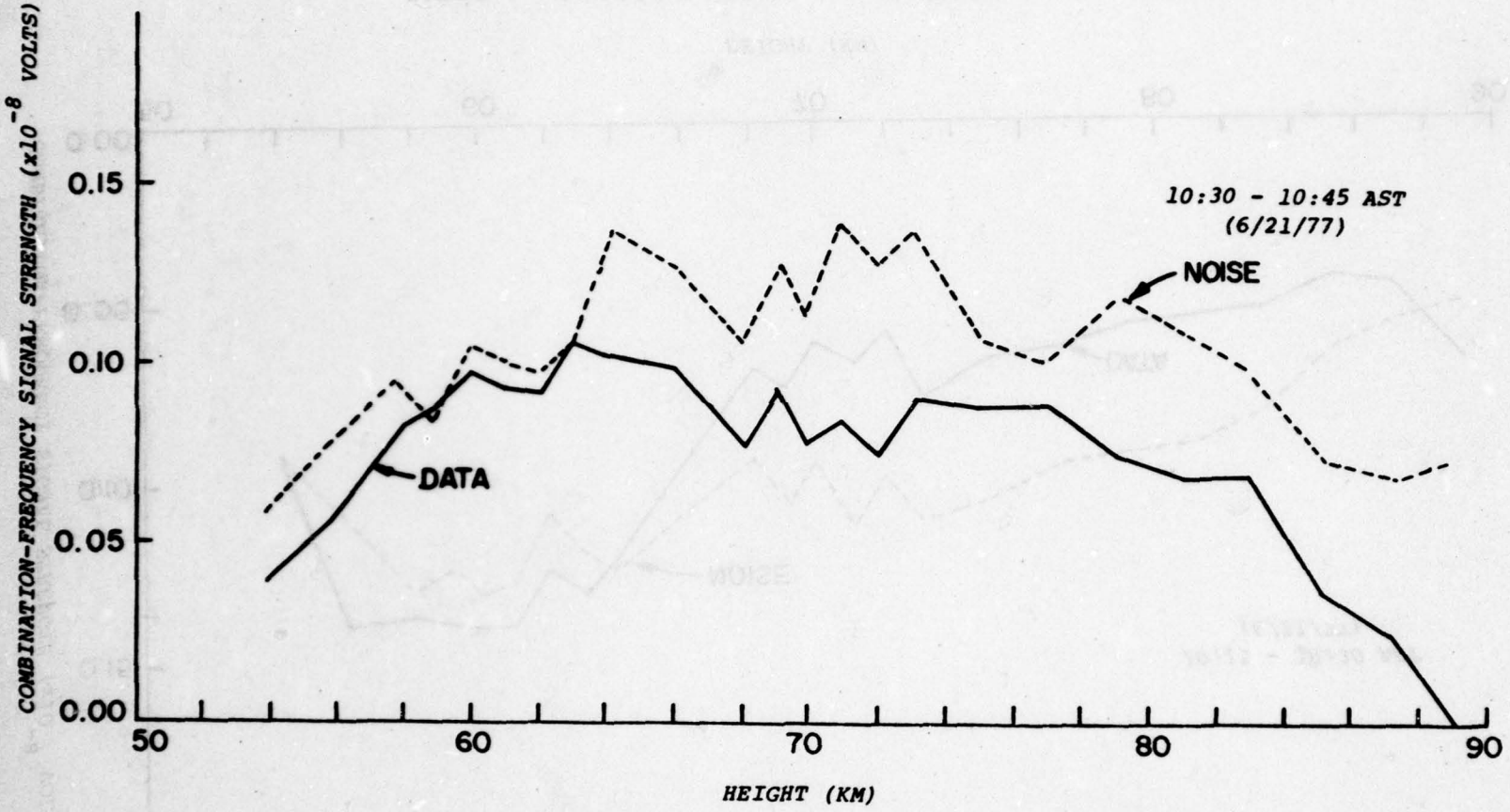

FIGURE 7: Combination-Frequency Signal Strength vs Height.

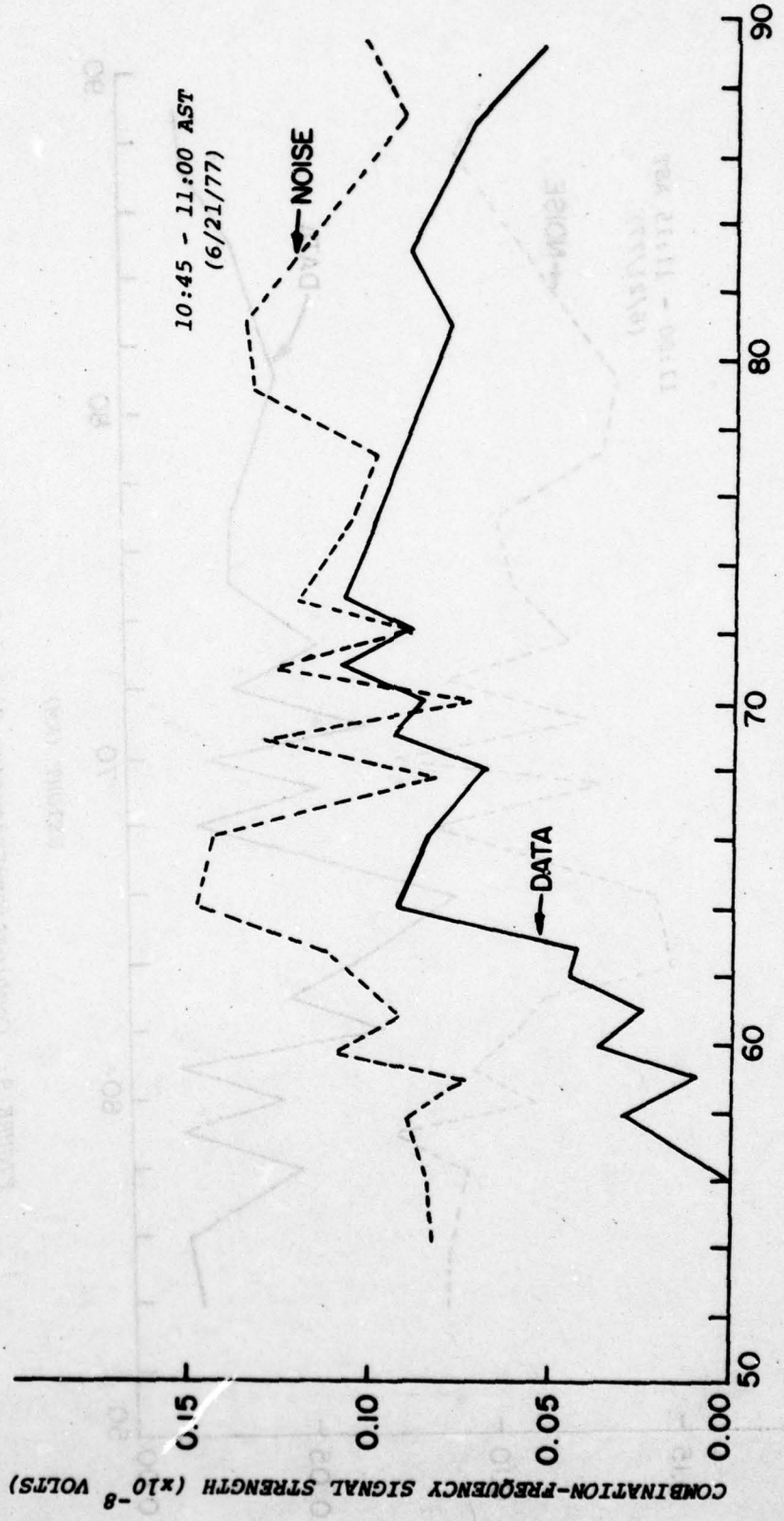

FIGURE 8: Combination-Frequency Signal Strength vs Height.

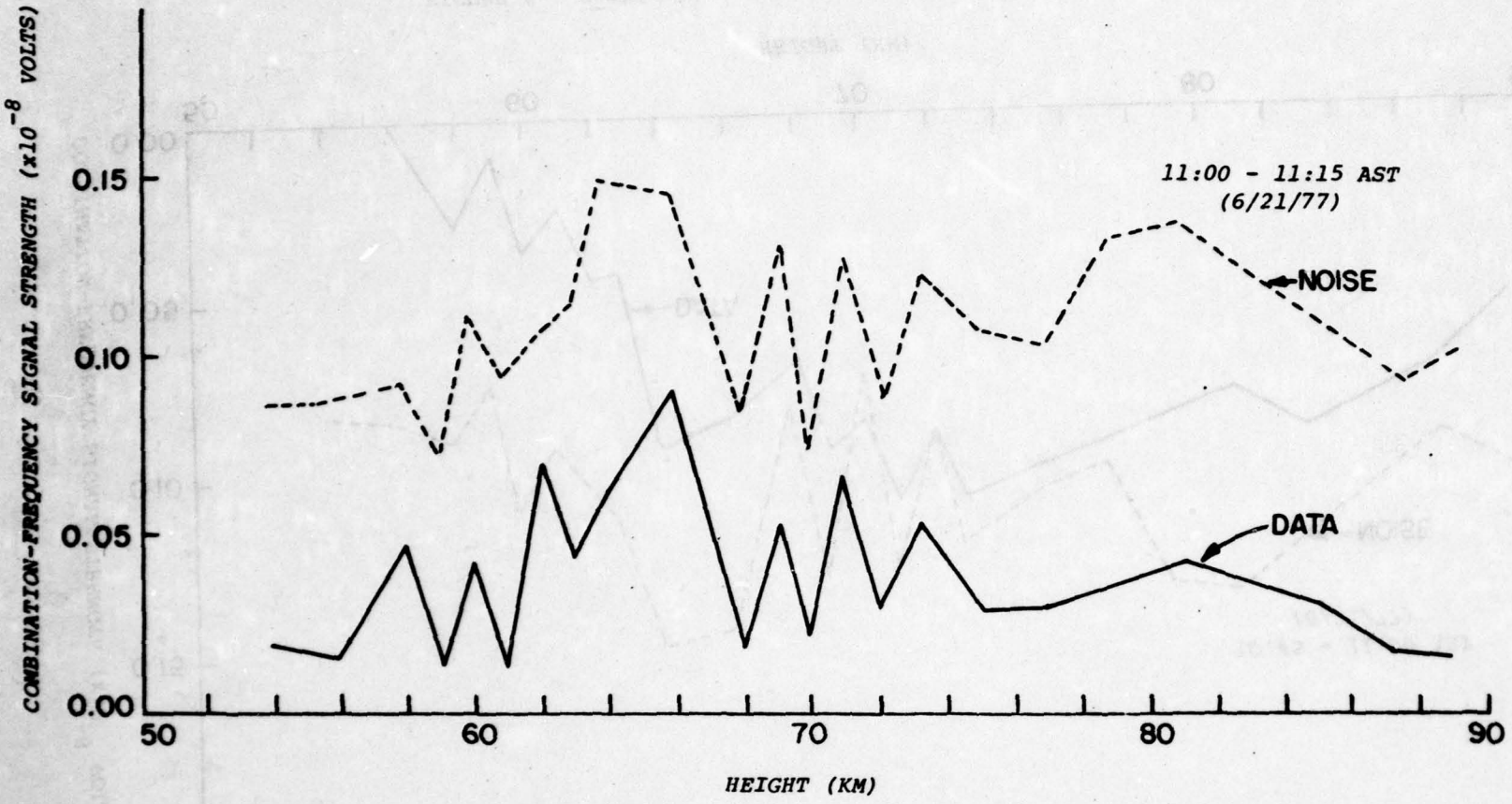

FIGURE 9: Combination-Frequency Signal Strength vs Height.

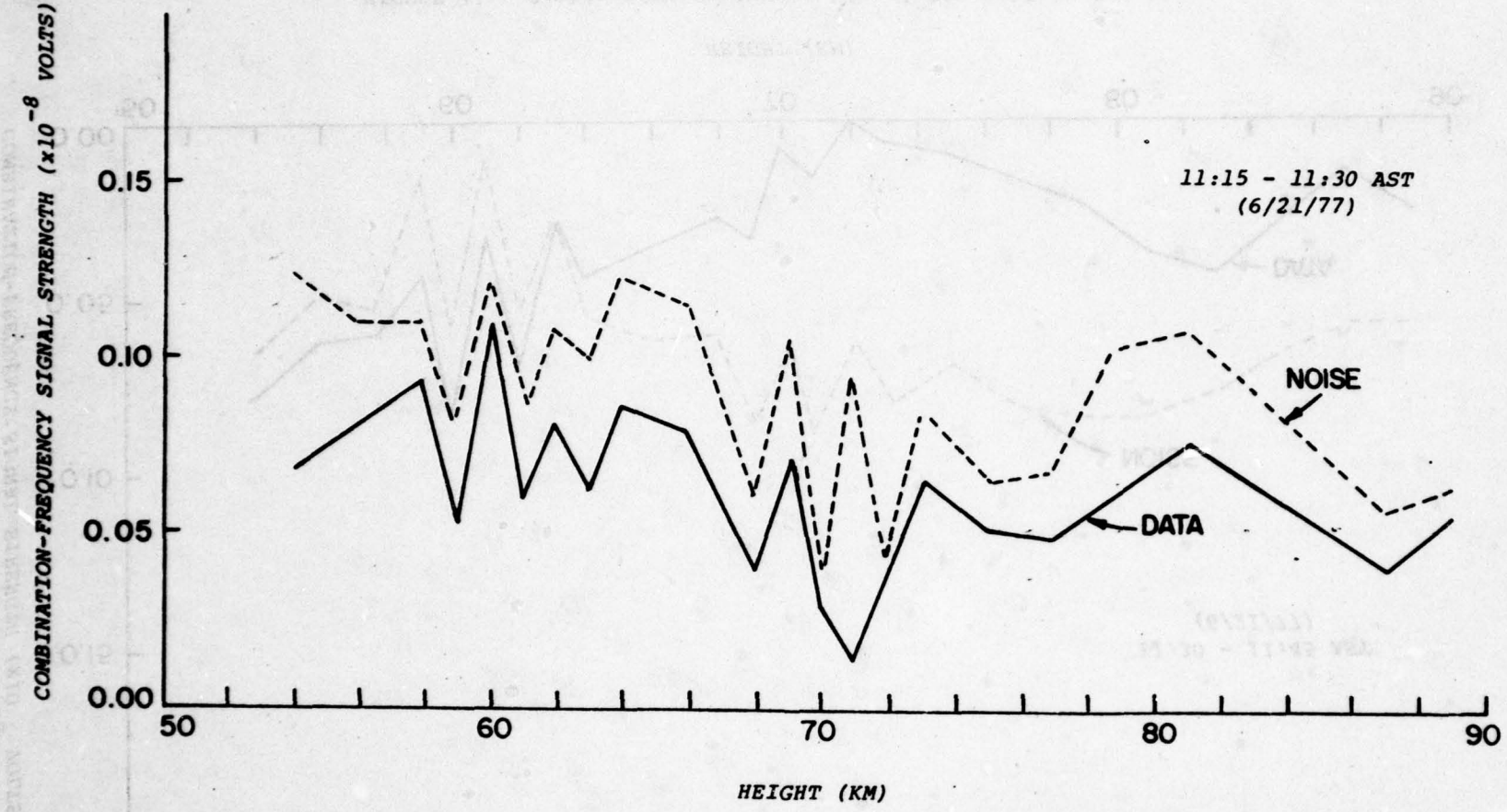

FIGURE 10: Combination-Frequency Signal Strength vs Height.

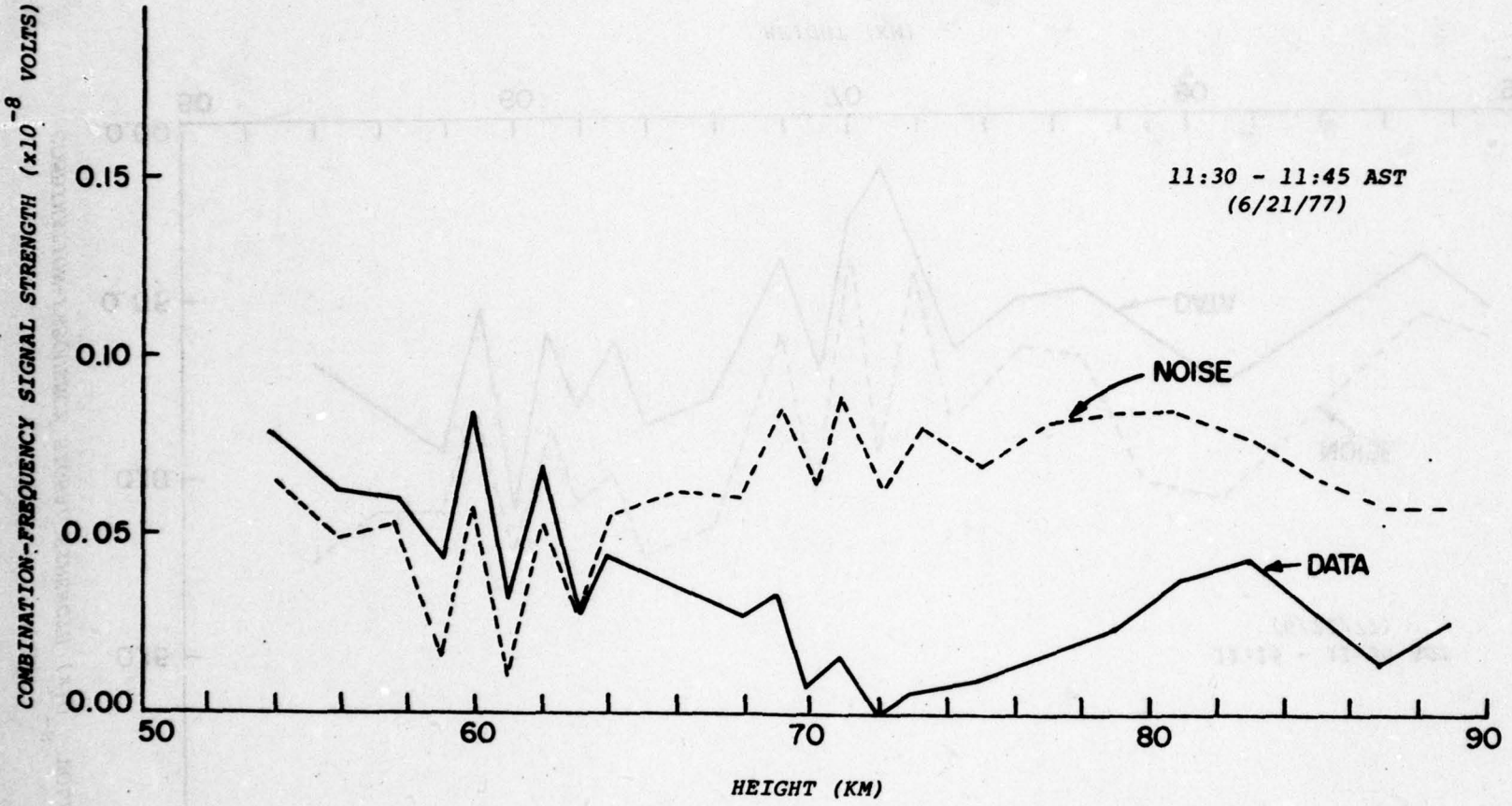

FIGURE 11: Combination-Frequency Signal Strength vs Height.

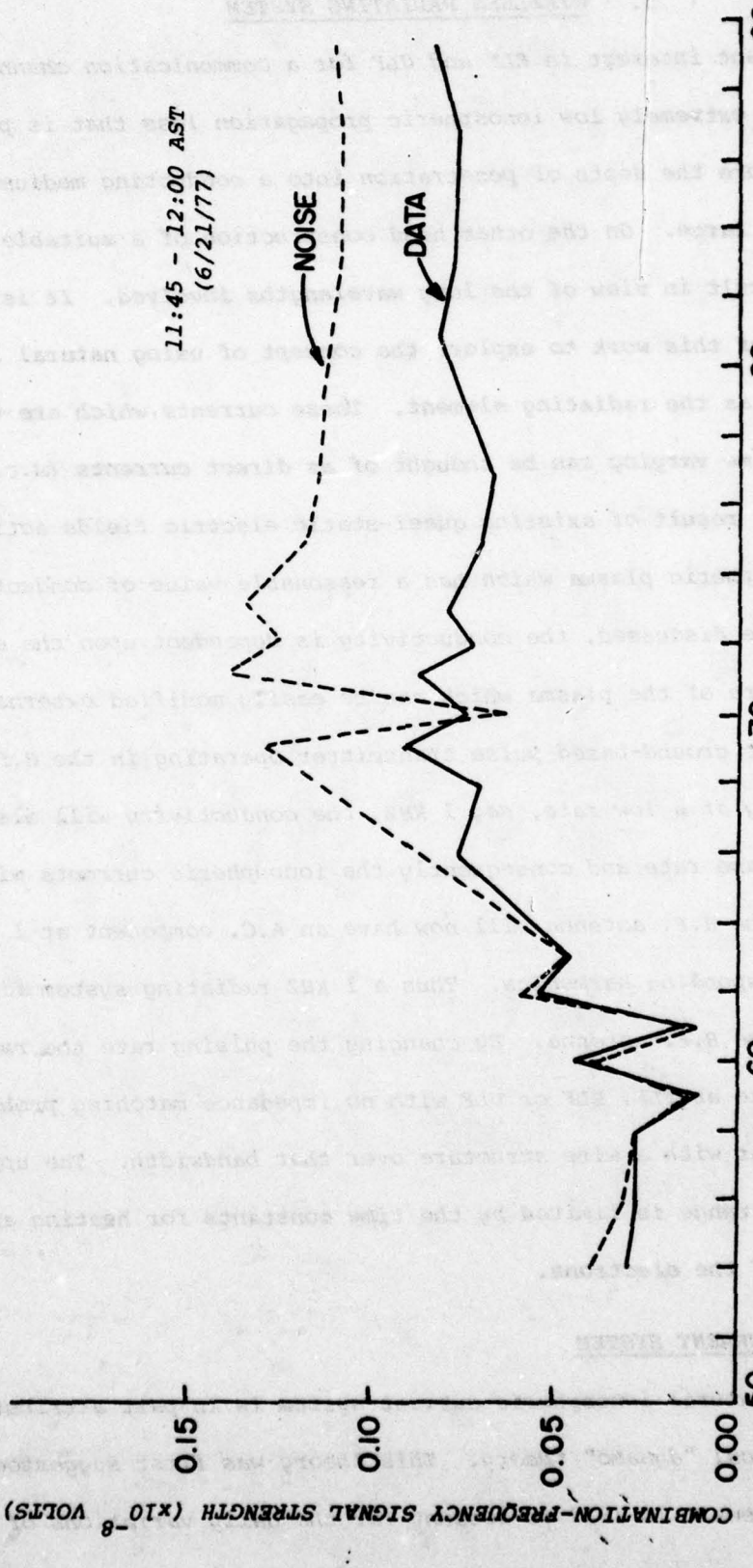

FIGURE 12: Combination-Frequency Signal Strength vs Height.

5. WIRELESS RADIATING SYSTEM

Recent interest in ELF and ULF for a communication channel results from the extremely low ionospheric propagation loss that is possible; furthermore the depth of penetration into a conducting medium like sea water is large. On the other hand construction of a suitable antenna is difficult in view of the long wavelengths involved. It is the purpose of this work to explore the concept of using natural ionospheric currents as the radiating element. These currents which are very slowly time varying can be thought of as direct currents (d.c.). They flow as a result of existing quasi-static electric fields acting upon the ionospheric plasma which has a reasonable value of conductivity. As will be discussed, the conductivity is dependent upon the electron temperature of the plasma which can be easily modified externally by a high power ground-based pulse transmitter operating in the H.F. band. By pulsing at a low rate, say 1 KHZ, the conductivity will also vary at this same rate and consequently the ionospheric currents within the beam of the H.F. antenna will now have an A.C. component at 1 KHZ and its corresponding harmonics. Thus a 1 KHZ radiating system fills the beam of the H.F. antenna. By changing the pulsing rate the radiator can operate at VLF, ELF or ULF with no impedance matching problems as would exist with a wire structure over that bandwidth. The upper frequency range is limited by the time constants for heating and cooling of the electrons.

5.1 THE CURRENT SYSTEM

The natural ionospheric current system is in part attributed to the classical "dynamo" theory. This theory was first suggested by Balfour Stewart in 1882 to account for the daily variations of the

geomagnetic field. The following summarized points about the dynamo theory are important:

1. The sun and moon produce tidal forces in the atmosphere, the periods being fractions of the solar day (24 hrs.) and lunar day (24.8 hrs.).

2. These forces set up standing waves in the atmosphere which results in primarily horizontal air motions. The atmosphere responds differently to forces of different periods.

3. The motion of the air across the geomagnetic field induces electromotive forces, which drive currents at levels where the electrical conductivity is appreciable (principally the E-region), thus causing the solar guiet-day and lunar magnetic variations.

4. Because of the vertical and horizontal variations of conductivity, currents cannot flow freely in all directions; polarization charges are thereby set up, modifying the flow of current.

5. Some order of magnitudes of quantities in the dynamo theory:

   i) induced electric field, $10^{-3} VM^{-1}$

   ii) current density, $10^{-6} AM^{-2}$

   iii) layer current density $10A\ KM^{-1}$

Recent USSR measurements of the vertical electric field summarized by Hale (1977) indicate a field of the order of $1\ VM^{-1}$ in the

stratosphere with some intensification in the mesosphere. If these electric field measurements are correct, then a vertical current system needs to be included into the ionospheric-antenna theory. This brings about exciting possibilities for creating an ionospheric antenna having both vertically and horizontally polarized far fields due to the vertical electric field and the horizontal "dynamo" induced electic field.

5.2 IONOSPHERIC CONDUCTIVITIES

The conductivity of the ionosphere is in fact defined by three conductivity terms:

i the longitudional conductivity σ_{ll}

ii the Pedersen conductivity σ_p

iii the Hall conductivity σ_H

The longitudional quantity σ_{ll} relates the current density J_{ll} to the electric field E_{ll} by

$$J_{ll} = \sigma_{ll} E_{ll}$$

when the electric field and the current density J_{ll} are along the Earth's magnetic field. The Pedersen value σ_p gives

$$J_p = \sigma_p E_\perp$$

where $E_\perp$ is the electric field perpendicular to the Earths' magnetic field lines and J_p is in the same direction as $E_\perp$. For the Hall conductivity, a current density J_H flows perpendicular to the applied field $E_\perp$ and perpendicular to the magnetic field lines;

$$J_H = \sigma_H E_\perp$$

Figure 13 shows the direction conventions for the three currents. The expressions for the conductivities in terms of ionospheric parameters as given by Ratcliffe[1972] are

$$\sigma_{11} = \frac{ne^2}{m\nu} \qquad (1)$$

$$\sigma_p = \frac{ne^2\nu}{m(\nu^2 + w_H^2)} \qquad (2)$$

$$\sigma_H = \frac{ne^2 W_H}{m(\nu^2 + W_H^2)} \qquad (3)$$

where n is the electron density

ν is the number of collisions per second of electrons with neutral particles

e is the electron charge

W_H is the electron angular gyrofrequency in the presence of the Earth's magnetic field.

Variation of these conductivity terms occur because of changes in electron temperature through the following relationships given by Banks and Kocharts [1973],

$$\nu_{N_2}(T_e) = 2.33 \times 10^{-11}\, n_{N_2}\, (1-1.2 \times 10^{-4}\, T_e)\, T_e \qquad (4)$$

$$\nu_{O_2}(T_e) = 1.8 \times 10^{-10}\, n_{O_2}\, (1+3.6 \times 10^{-2} T_e^{1/2})\, T_e^{1/2} \qquad (5)$$

where

ν_{N_2}, ν_{O_2} are the collisional rates of electrons with species N_2, O_2

n_{N_2}, n_{O_2} are the densities of the species N_2 and O_2

T_e is the electron temperature in degrees Kelvin

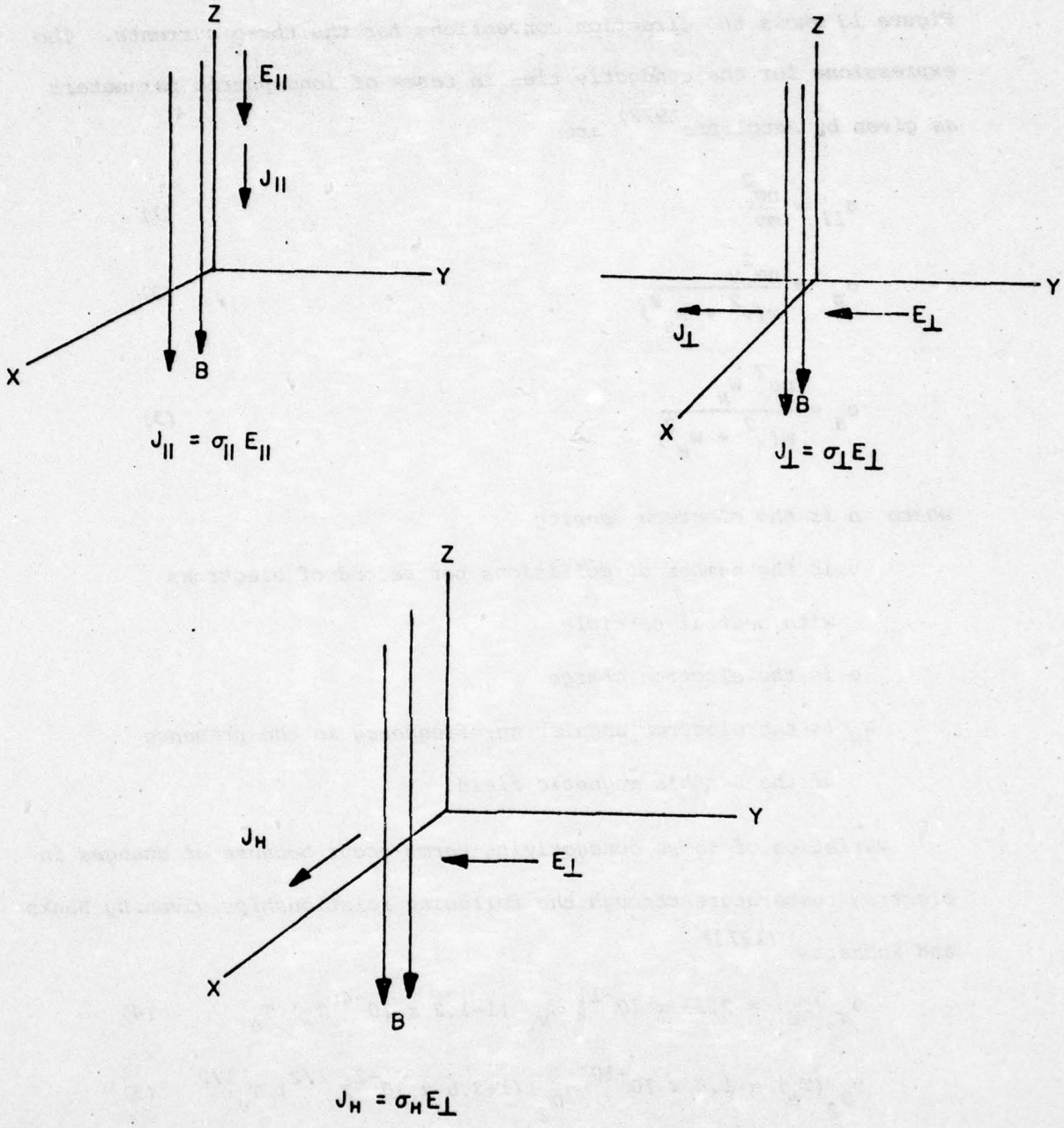

FIGURE 13 Direction Conventions for Current Density Flow in Terms of the Three Ionospheric Conductivity Terms

Thus if one can externally change the electron temperature with time, $\Delta T_e(t)$, then there results a change in ionospheric current with time, $\Delta J(t)$, since

$$\Delta J(t) = \frac{\partial \sigma}{\partial T_e} \Delta T_e(t) \qquad (6)$$

If $\Delta T_e(t)$ is periodic, the periodic $\Delta J(t)$ will radiate electromagnetic waves with those frequencies contained in the spectrum of $\Delta T_e(t)$. If electron temperature changes are large enough, then not only will the collision frequency be modified but so can the electron density change due to variations in the chemistry which is temperature dependent. Then it is necessary to rewrite (6) as

$$\Delta J(t) = \left(\frac{\partial \sigma}{\partial \nu} \frac{\Delta \nu}{\Delta T_e} + \frac{\partial \sigma}{\partial n} \frac{\Delta n}{\Delta T_e} \right) \Delta T_e(t)\, E \qquad (7)$$

5.3 IONOSPHERIC HEATING

The differential expression relating electron temperature to R.F. heating is simply

$$\frac{3}{2} n K_B \frac{\partial T_e}{\partial t} = P_e + \sum_i \left(\frac{dU_e}{dt} \right)_i \qquad (8)$$

where T_e = electron temperature

n = electron density

K_B = Boltzmann's constant

P_e = rate of electron thermal energy production transferred to the electrons by R.F. heating.

$\left(\frac{dU_e}{dt} \right)_i$ = rate of electron thermal energy loss due to the i^{th} type of electron-neutral collisional process.

The types of electron energy loss processes responsible for cooling of electrons are elastic and inelastic collisions and the latter are more effective in cooling electrons. The various kinds of inelastic cooling rates are due to excited rotational states of N_2 and O_2 and excited vibrational states of N_2.

Now to find the expression for P_e one needs to find the local power density, S, at height h within the cone illuminated by an R.F. source radiating at frequency f. This is given by the usual attenuation equation for a spherical wave front,

$$S(h) = S_o \left(\frac{h_o}{h}\right)^2 \exp\left\{-2k_o \int_{h_o}^{h} \chi(h^1)\,dh^1\right\} \qquad (9)$$

where $S_o = \dfrac{P_T G}{4\pi h_o^2}$ is the power density at some reference height h_o below the base of the ionosphere

P_T = R.F. transmitter power

G = gain of the antenna over isotropic source

k_o = free space propagation constant

$\chi(h)$ = ionospheric absorption index at height h

now

$$\frac{\partial S(h)}{\partial h} = -\frac{2}{h} S(h) - 2 k_o \chi(h)\, S(h) \qquad (10)$$

The first term on the right accounts for the decrease in power density because of the increasing surface area of the expanding spherical wave while the second term represents the energy dissipation per unit volume in the ionosphere as a result of absorption by electrons. One, therefore, writes

$$P_e(h) = -\left.\frac{\partial S(h)}{\partial h}\right|_{\text{due to absorption}} = 2 k_o \chi(h)\, S(h) \qquad (11)$$

Equation (11) must be substituted into the energy balance equation (8).

Since $\chi(h)$, the absorption index, is function of collision frequency, it is expected that it will vary with T_e and so will $S(h)$. Thus to find a complete time history of T_e, one needs to solve equation (8) simultaneously with equation (10). These equations are rewritten to show the coupling because of electron temperature changes.

$$\frac{\partial S(h,T_e)}{\partial h} = -\frac{2}{h} S(h, T_e) - 2 k_o \chi(h, T_e) S(h, T_e) \quad (12)$$

$$\frac{\partial T_e(h)}{\partial t} = \frac{2}{3K_B n(h)} \left[2 k_o \chi(h, T_e) S(h, T_e) + \sum_i \left(\frac{dU_e(h,T_e)}{dt}\right)_i \right] \quad (13)$$

Equations (12) and (13) have been solved for an electromagnetic pulsed value of S_o and the resulting time history of T_e used to calculate the changes in the conductivities given by (1), (2), and (3). Consequently, one can evaluate $\Delta J_p(t)$, $\Delta J_H(t)$ and $\Delta J_{11}(t)$. This is done in the next section and radiated powers are found.

5.4 NUMERICAL RESULTS OF PREDICTED RADIATED POWERS BELOW 10KHZ

This section presents calculations of the radiated powers of the longitudional, Hall and Pedersen current systems for a typical mid-day D-region (Lee and Ferraro - 1969) with ambient collision frequencies calculated from the neutral densities and ambient neutral temperatures from the CIRA (1972) Mean Reference Atmosphere. A value of 100 megawatts of effective radiated power is used with extraordinary mode heating at 5.0 MHZ. A half-power beamwidth of 20° is assumed. A pulse rate of 10 KHZ and 1 KHZ with 50% duty cycle and ideal rectangular shape is

used; thus with these parameters, equations (12) and (13) were solved numerically to give $T_e(h,t)$. Table I tabulates these results for the altitude range of 60 to 90 km. Only the temperature at the end of the heating cycle is given here (50 μs for 10 KHZ and 0.5 MS for 1 KHZ) as this will specify the maximum change in current at each altitude. As seen greater temperatures are attained with the 1 KHZ pulse rate since equilibrium is more easily reached because of the longer heating period of 0.5 ms. From these temperature results, the collision frequencies of equations (4) and (5) allow the computation of the conductivities given by (1), (2), and (3). Figures 14, 15, and 16 show the altitude dpendence of σ_{11}, σ_p, and σ_H respectively for ambient conditions, 10 KHZ and 1 KHZ pulsed conditions. Thus significant changes in the conductivity of the ionosphere can be made below 80 km. Although the conductivities are greater above 90 km and the dynamo current will be large there, larger changes in current can occur only in the D-region due to heating. Again, it is the change in current that is responsible for the radiation. Actually, it is necessary to Fourier analyze the periodic $\Delta J(t)$ in order to find the A.C. components and the radiated power at each frequency component. In the work which follows we simply use 1/2 of ΔJ_{MAX} as the amplitude of the 10 KHZ or 1 KHZ component.

Table II tabulates the changes in conductivity versus altitude for 1 KHZ and 10 KHZ; the units are in micro-mhos per meter. At 1 HZ, one simply uses the 1 KHZ values as the conductivity has reached essentially maximum change at most heights for the 0.5 MS heating time. To estimate a numerical value for the radiated power certain approximations are used in this preliminary work. The "heater" antenna beam is idealized as

TABLE 1 Electron Temperature vs. Altitude for 1 KHZ and 10 KHZ

h (KM)	(ambient) T_n (^oK)	(0.5 ms) T_e (^oK)	(50 μs) T_e (^oK)
60	249.3	407.9	406.1
61	246.0	429.3	425.5
62	242.7	454.5	447.0
63	239.4	483.9	470.1
64	236.1	518.0	494.1
65	232.7	557.0	517.8
66	229.0	600.0	539.2
67	225.5	648.5	558.1
68	222.2	702.8	572.6
69	219.1	760.6	579.5
70	216.2	817.5	574.2
71	213.7	869.5	554.0
72	211.3	912.8	519.9
73	209.1	943.6	476.7
74	207.0	959.4	430.1
75	205.0	956.1	385.6
76	203.0	926.1	347.3
77	201.0	862.7	316.5
78	198.9	771.2	291.0
79	196.9	661.6	267.7
80	194.9	549.5	251.2
81	192.9	458.7	236.1
82	190.9	391.9	225.3
83	188.8	344.3	215.3
84	186.9	307.8	208.3
85	184.9	280.3	201.3
86	184.6	259.5	197.7
87	184.2	242.5	194.1
88	183.9	230.2	191.3
89	183.6	219.2	189.4
90	183.4	210.8	187.7

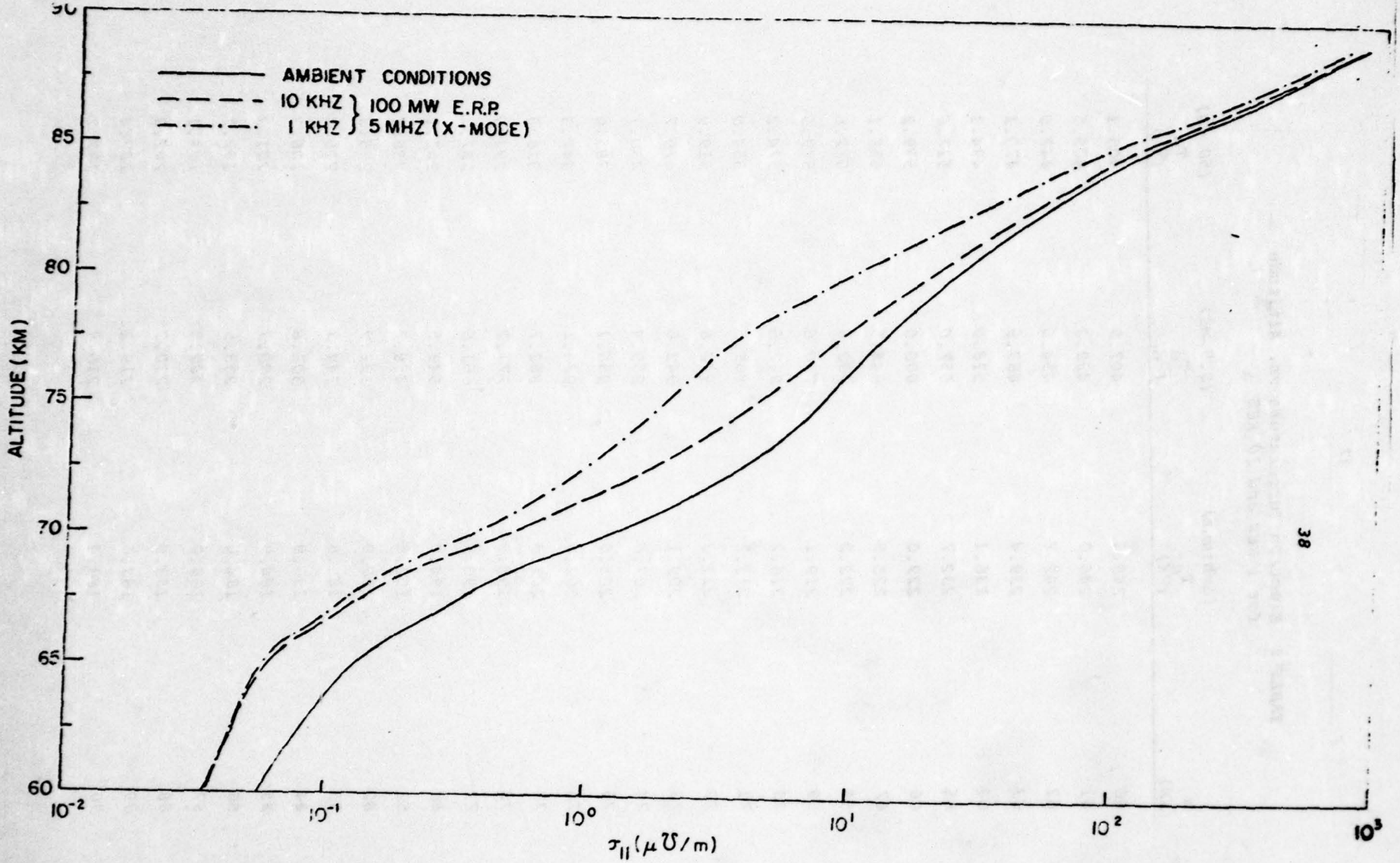
AMBIENT CONDITIONS
10 KHZ } 100 MW E.R.P.
1 KHZ } 5 MHZ (X-MODE)
ALTITUDE (KM)
90
85
80
75
70
65
60
10^{-2}
10^{-1}
10^{0}
10^{1}
10^{2}
10^{3}
τ_{11} (μ U/m)

FIGURE 14

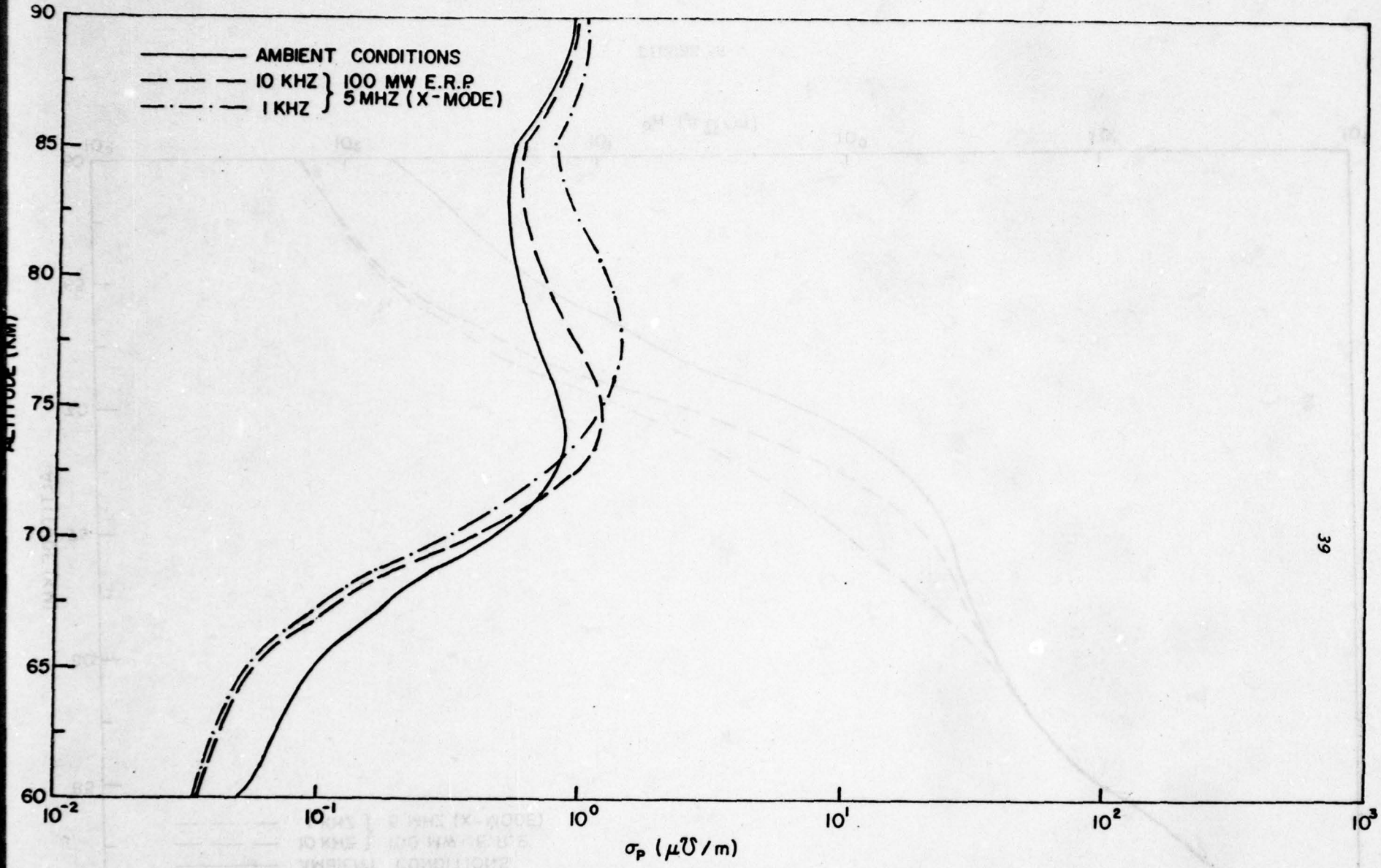
AMBIENT CONDITIONS
10 KHZ
1 KHZ
100 MW E.R.P
5 MHZ (X-MODE)
90
85
80
75
70
65
60
ALTITUDE (KM)
10^{-2}
10^{-1}
10^{0}
10^{1}
10^{2}
10^{3}
σ_p ($\mu\mho$/m)

FIGURE 15

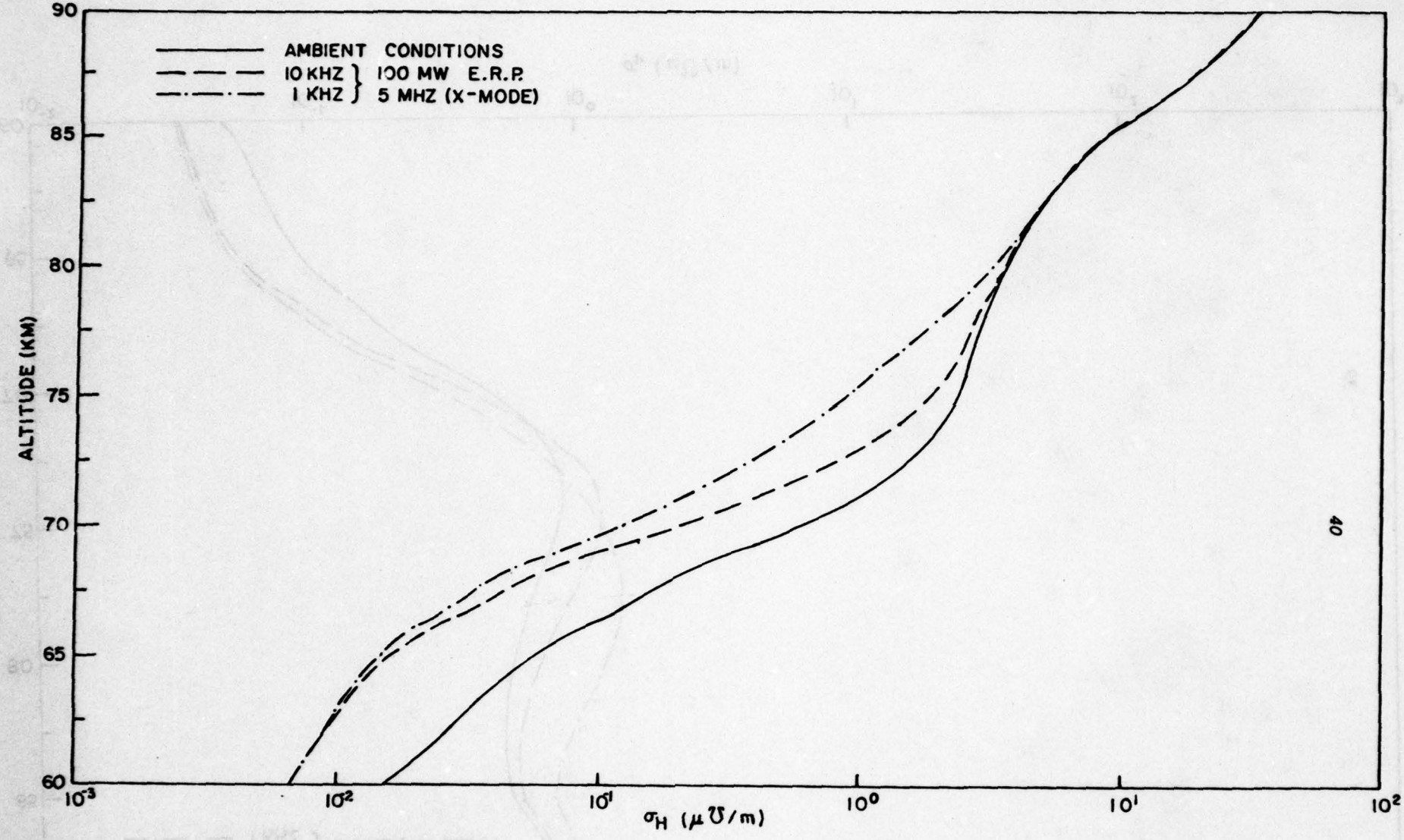
AMBIENT CONDITIONS
10 KHZ } 100 MW E.R.P.
1 KHZ } 5 MHZ (X-MODE)
ALTITUDE (KM)
90
85
80
75
70
65
60
10^{-3}
10^{-2}
10^{-1}
10^{0}
10^{1}
10^{2}
σ_H (μ ℧/m)
40

FIGURE 16

TABLE II Changes in Conductivity Versus Altitude for 1 KHZ and 10 KHZ Pulse Rates at 50 Percent Duty Cycle

	← 1 KHZ →			← 10 KHZ →		
km	$\Delta\sigma_H$	$\Delta\sigma_{11}$	$\Delta\sigma_p$	$\Delta\sigma_H$	$\Delta\sigma_{11}$	$\Delta\sigma_p$
60	8.5E-3	1.0E-2	1.6E-2	8.5E-3	1.0E-2	1.5E-2
65	4.5E-2	4.5E-2	4.2E-2	3.9E-2	4.5E-2	3.7E-2
70	4.97E-1	6.7E-1	1.7E-1	4.0E-1	7.0E-1	7.0E-2
75	1.45E-0	5.4E-0	-1.7E-1	8.0E-1	3.4E-0	-3.5E-1
80	4.0E-1	1.48E+1	-4.5E-1	0	8.0E-0	-1.6E-1
85	0	1.3E+1	-2.5E-1	0	1.0E+1	-5.0E-2

TABLE III Parameters Used in Approximate Calculation of Radiated Powers for Geometry Shown in Figure 17

	10 KHZ	1 KHZ	1 HZ
ℓ	26 km	26 km	26 km
ΔX	26 km	26 km	26 km
ΔZ	5 km	5 km	5 km
$\Delta\sigma_H$	8×10^{-1} μ MHO/M	1.45×10^{0}	1.45×10^{0}
$\Delta\sigma_p$	3.5×10^{-1} μ MHO/M	4.5×10^{-1}	4.5×10^{-1}
$\Delta\sigma_{11}$	1.0×10^{1} μ MHO/M	1.48×10^{1}	1.48×10^{1}
Z_{max}	≈80 km	≈75 km	≈75 km
E_{Dynamo}	25 mv-M^{-1}	25 mv-M^{-1}	25 mv-M^{-1}
$E_{Vertical}$	0.1 V-M^{-1}	0.1 V-M^{-1}	0.1 V-M^{-1}
$R_{p,H}$	* 121 Ω	5.93 Ω	5.93×10^{-6} Ω
R_{11}	** 3.2 Ω	0.2 Ω	$.2 \times 10^{-6}$ Ω
W_H	204 w	33 w	33 μw
W_p	38 w	3 w	3 μw
W_{11}	454 kw	50 kw	5 mw

* See Appendix A

** See Appendix B

shown in Figure 17 and the Earth's field is taken as vertical (actually it is 19° from the vertical at University Park). The maximum change in conductivity occurs near 75 or 85 km; it is assumed that this maximum change occurs in a slab of vertical thickness of 5 km and the changes outside this region are ignored. This geometry is shown in Figure 17 for both the horizontal and vertical current system. The parameters for this geometry are tabulated under Table III. For 1 KHZ and 1 HZ the radiation is considered to be a short dipole (horizontal or vertical) with uniform current distribution; this is greatly in error at 10 KHZ for dimension "ℓ" is close to one wavelength. Where the short dipole approximation is used, the standard radiation resistance formula can be applied:

$$R = 80\pi^2 \left(\frac{h}{\lambda}\right)^2 \qquad (14)$$

where $h = \ell$ for horizontal current or $h = \Delta Z$ for vertical currents. At 10 KHZ, Appendices 1 and 2 derive the necessary radiation resistances unique to the specific geometries. These values are given in Table III. Final computed radiated powers W_H, W_p, and W_{ll} for Hall, Pedersen, and parallel current systems respectively are the last three items in the table. The large values for W_{ll} reflect the postulated large vertical electric field compared to the horizontal "dynamo" electric field. Actually ΔJ is a function of all three space coordinates, i.e. $\Delta J(X,Y,Z)$ due to the spatial variation of "heater" power density which was ignored in this analysis. Furthermore $\Delta J(Z)$ has associated with it a phase shift since there is a time delay of about 150 μs for propagation of the heater signal to reach 90 km from a reference height of 40 km. It is thus expected that the 10 kHZ radiated power would not be as large as given in Table III. These preliminary results do warrant further experimental and theoretical research programs.

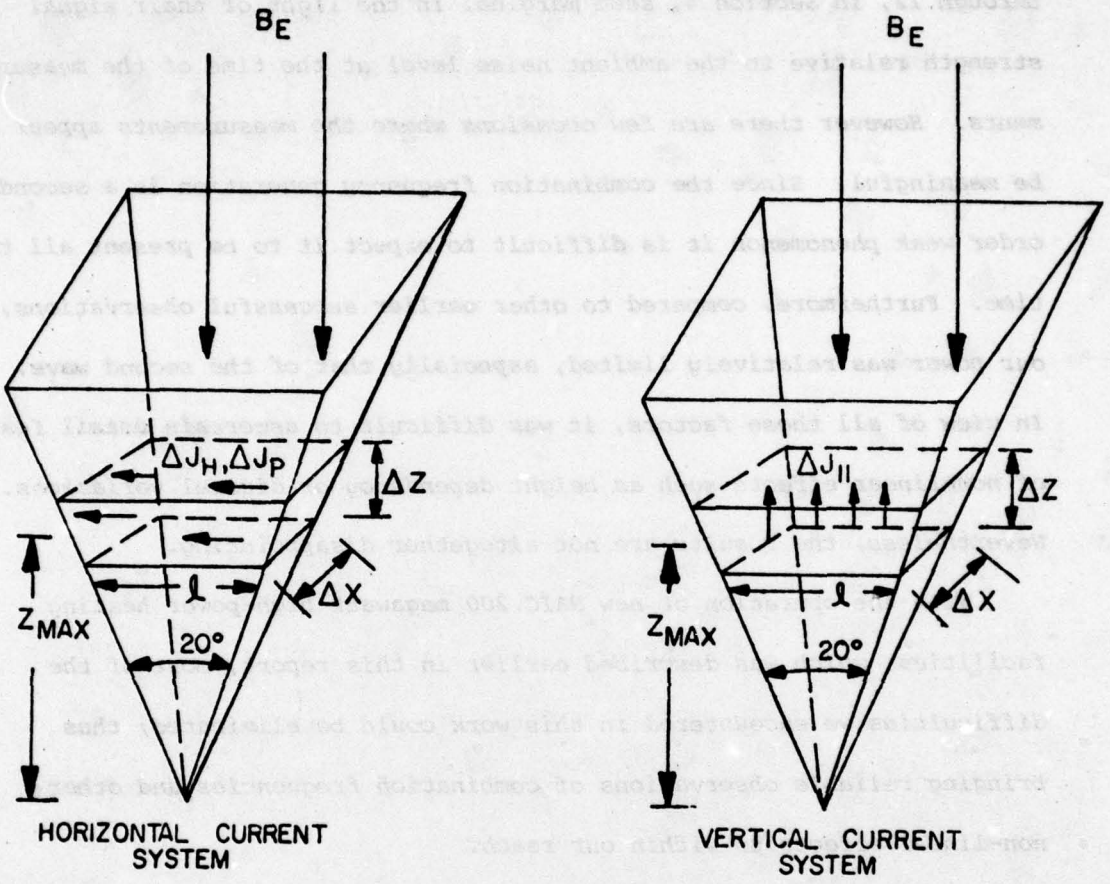

FIGURE 17: *Idealized Geometry of Radiating Elements for Horizontal and Vertical Currents*

6. DISCUSSIONS

The results of combination frequency measurement shown in Figures 3 through 12, in Section 4, seem marginal in the light of their signal strength relative to the ambient noise level at the time of the measurements. However there are few occasions where the measurements appear to be meaningful. Since the combination frequency generation is a second order weak phenomenon it is difficult to expect it to be present all the time. Furthermore, compared to other earlier successful observations, our power was relatively limited, especially that of the second wave. In view of all these factors, it was difficult to ascertain detail features of non-linear effects such as height dependency or diurnal variations. Nevertheless, the results are not altogether disappointing.

With the operation of new NAIC 200 megawatt high-power heating facilities, which was described earlier in this report, most of the difficulties we encountered in this work could be eliminated; thus bringing reliable observations of combination frequencies and other non-linear effects to within our reach.

Theoretical analysis of the wireless radiating system presented in Section 5 explored the feasibility of using the modulated ionospheric current system to alleviate the difficulty of constructing extremely long antenna system in ELF or ULF communications. Initial numerical results on the powers radiating from the system certainly support the feasibility of this concept. It will undoubtedly be a worthwhile endeavor to test this concept experimentally using the new NAIC high-power facilities at Arecibo in the future.

Appendix A. Calculation of R_p and R_H and radiated powers for 10 KHZ for Horizontal Current Density

Figure A.1 reproduces the geometry of the current carrying region idealized in Figure 17; ΔJ_p or ΔJ_H is parallel to the y axis. The surface of this square slab of dimension ℓ is divided into a large number of small isotropic radiators of dimensions Δx and Δy. The radiation pattern of a square array of isotropic radiators can be shown to have the following form by using the classical pattern multiplication theorem:

$$\text{pattern} = \frac{\ell^2}{\Delta x \Delta y} \frac{\text{Sin}\left(\frac{\pi \ell}{\lambda} \text{ Sin } \theta \text{ Cos } \phi\right)}{\frac{\pi \ell}{\lambda} \text{ Sin } \theta \text{ Cos } \phi} \frac{\text{Sin}\left(\frac{\pi \ell}{\lambda} \text{ Sin } \theta \text{ Sin } \phi\right)}{\frac{\pi \ell}{\lambda} \text{ Sin } \theta \text{ Sin } \phi} \qquad \text{(A-1)}$$

This then is multiplied by the electric field equation for a short dipole since each elementary aperature $\Delta x \Delta y$ shown in Figure A.1 can be considered a short dipole of length Δy and cross-section $\Delta x \Delta z$. The current in this dipole is $\Delta J_p \Delta x \Delta z$ or $\Delta J_H \Delta x \Delta z$. The standard equation for field strength of this short dipole becomes in free space

$$E_\theta = \frac{60\pi \Delta y \quad (\Delta J \Delta x \Delta z) \text{ Sin } \psi}{\lambda R} \qquad \text{(A-2)}$$

where

$$\text{Sin } \psi = \left[1 - \text{Sin}^2 \theta \text{ Sin}^2 \phi\right]^{1/2} \qquad \text{(A-3)}$$

From (A-1), (A-2) and (A-3), the free space Poynting vector can be found and integrated over a sphere to find the total radiated power and consequently the radiation resistance. The final result can be expressed as:

$$W = \frac{120\pi \ell^2 I^2}{\lambda^2} \int_0^{90^\circ} \int_0^{90^\circ} f_1^2(\theta, \phi) \left(\frac{\text{Sin } v}{v}\right)^2 \left(\frac{\text{Sin } v}{v}\right)^2 d\theta d\phi \qquad \text{(A-4)}$$

where $I = (\Delta J \ell \Delta z)$

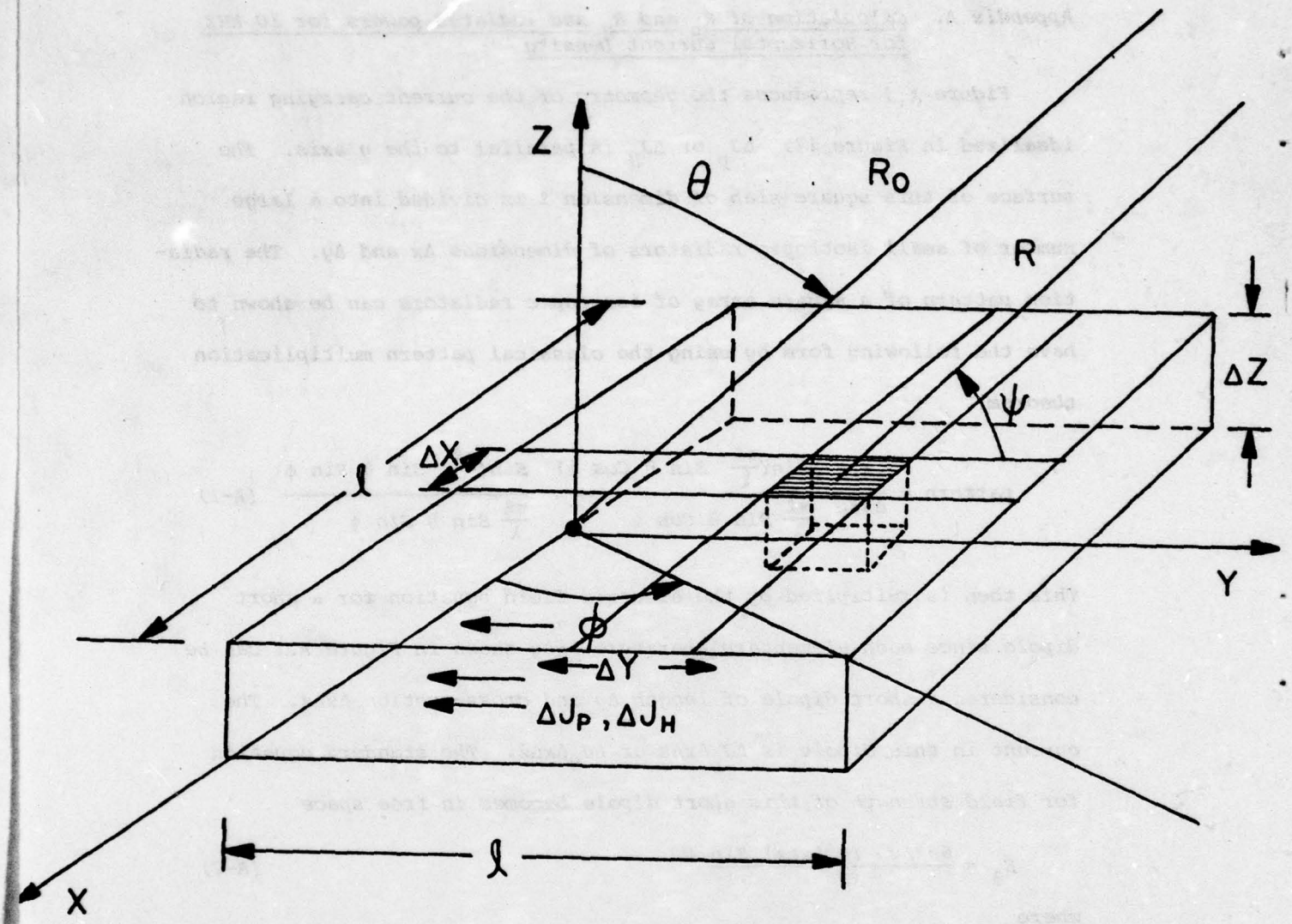

FIGURE A.1: The current carrying region of the geometry shown in Figure 17.

$$f_1^2(\theta,\phi) = \sin\theta\,(1 - \sin^2\theta\sin^2\phi)$$

$$\nu = \frac{\pi\ell}{\lambda}\sin\theta\cos\phi$$

$$v = \frac{\pi\ell}{\lambda}\sin\theta\sin\phi$$

At 10 KHz, $\frac{\ell}{\lambda} \approx 1$. Equation (A-4) was integrated numerically using 36 points over one octant of the sphere. The final result is

$$W = 60.55\, I^2 \qquad \text{(A-5)}$$

Since I is defined as the peak A.C. current, the radiation resistance becomes

$$R_p = R_H = 121\ \Omega$$

Appendix B. Calculation of R_H and Radiated Power from a Disk at 10 KHz Carrying a Uniform Vertical Current Density

In Figure B.1, the "heater" beam is represented as a cone rather than an inverted pyramid as in Figure 17 to facilitate the integration. The disk represent the dominant current carrying region.

Each axial current radiates as a small dipole; if $\Delta z/\lambda$ is small according to the usual small dipole field

$$E_\theta = \frac{(\Delta J_{11})(\Delta z) R^1 d\phi^1 dR^1 jw\mu e^{-jkR}}{4\pi R} \text{ Sin } \theta \qquad \text{(B-1)}$$

subject to the far field approximation

$$R = R_o - R^1 \text{Sin } \theta \text{ Cos}(\phi - \phi^1) \qquad \text{(B-2)}$$

the resultant far electric field becomes

$$E = \frac{(\Delta J_{11})\ (\Delta z) jw\mu \text{ Sin } \theta e^{-jkR_o}}{4\pi R_o} \int_{\phi^1=0}^{2\pi} \int_{R^1=0}^{a} e^{jkR^1 \text{ Sin } \theta \text{ Cos}(\phi-\phi^1)} R^1 dR^1 d\phi^1 \qquad \text{(B-3)}$$

Integrating over ϕ^1 first, the magnitude of E becomes

$$/E/ = \frac{(\Delta J_{11})\ (\Delta z) w\mu \text{ Sin } \theta\ 2\pi}{4\pi R_o} \int_0^a J_o(kR^1 \text{ Sin } \theta)\ R^1\ dR^1 \qquad \text{(B-4)}$$

Equation (B-4) was arrived at by using the Bessel function representation

$$2\pi J_o(q) = \int_o^{2\pi} e^{jq \text{ Cos } \phi^1}\ d\phi^1 \qquad \text{(B-5)}$$

Now employing the identity

$$\int X\ J_o(x) dX = X J_1(x) \qquad \text{(B-6)}$$

one can obtain for free space

$$/E/ = \frac{60I}{R_o}\ \left(\frac{\Delta z}{a}\right)\ J_1\ (ka \text{ Sin } \theta) \qquad \text{(B-7)}$$

where $I = (\Delta J_{11})\ (\pi a^2)$

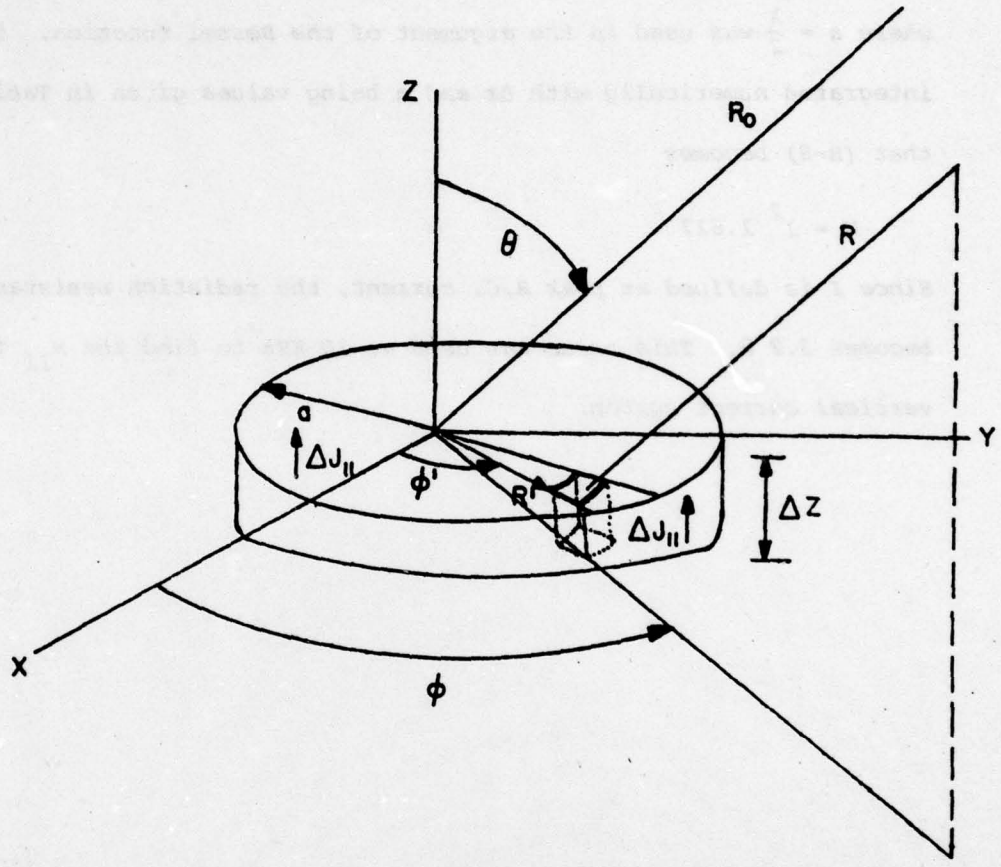

FIGURE B.1: A current carrying disk which replaces the current carrying region of Figure 17.

Integrating numerically the Poynting vector corresponding to (B-7), the radiating power becomes

$$W = 60I^2 \int_0^{90^\circ} \left(\frac{\Delta z}{a}\right)^2 \text{Sin}\,\theta \quad [J_1\,(\pi \text{Sin}\theta)^{\,2}] \qquad \text{(B-8)}$$

where $a = \frac{\lambda}{2}$ was used in the argument of the Bessel function. This is integrated numerically with Δz and a being values given in Table I so that (B-8) becomes

$$W = I^2\ 1.617 \qquad \text{(B-9)}$$

Since I is defined as peak A.C. current, the radiation resistance becomes 3.2 Ω. This value was used at 10 KHz to find the W_{11} for the vertical current system.

REFERENCES

Bailey, V. A., "On Some Effects Caused in the Ionosphere by Electric Waves", Phil. Mag., 23, 929, 1937.

Banks, P. M. and G. Kockarts, Aeronomy, Part B, Academic Press, 1973, Chapter 22.

Cutolo, M., "On Some New Properties of the Lower Ionosphere", in "Propagation of Radio Waves at Frequencies Below 300 kc/s", W. T. Blackband, Editor, Pergamon Press.

Getmantsev, G. G., Zuikov, N. A., Kotik, D. S., Mironenko, L. F., Mityakov, N. A., Rapoport, V. O., Sazanov, Yu A., Trakhtengerts, V. Yu., and Eidman, V. Ya., "Combination Frequencies in the Interaction between High-power Short-wave Radiation and Ionospheric Plasma", ZhETF Pis. Red. 20, 229-232, 1974.

Ginzburg, V. L., and Gurevich, A. V., "Non-Linear Phenomena in a Plasma Located in an Alternating Electromagnetic Fields", Sov. Phys. Usp. 3, 115-146 and 175-194, 1960.

Hale, L. C., "Particle Transport Through the Mesosphere and Stratosphere", Nature, 268, p. 710, August 5, 1977.

Lavergnat, J., Bauer, P., Delahaye, J. Y. and Ney, R., "Non-Linear Sounding of the Ionospheric Plasma", Private Communication, 1977.

Lee, H. S. and A. J. Ferraro, "Winter D-Region Electron Density and Collision Frequency Features Obtained with High-Power Interaction Measurements", J. Geophys. Res., 74(5), March 1, 1969.

Mityakov, N. A., V. O. Rapoport and V. Yu Trakhtengerts, "Experimental Investigations of Non-Linear Effects in the F-Layer of the Ionosphere", Radiofizika, 19(1), 33-42, January, 1976.

Ratcliffe, J. A., An Introduction to the Ionosphere and Magnetosphere, Cambridge University Press, 1972, Chapter 7.

Distribution List for Pennsylvania State University
Final Report
21 February 1979

ONR Branch Office

Office of Naval Research
495 Summer Street
Boston, Mass. 02210

1 cy

ACO

ONR Resident Representative
Carnegie-Mellon University
Room 407 Margaret Morrison Bldg.
Pittsburgh, Pa. 15213

1 cy

Department of Defense

Director
Defense Advanced Research Projects Agency
1400 Wilson Boulevard
Arlington, Virginia 22209

1 cy ATTN: TIO
1 cy ATTN: STO
1 cy ATTN: NRMO

Director
Defense Communications Agency
8th Street and South Courthouse Road
Arlington, Virginia 22204

3 cys ATTN: MEECN Office

Defense Documentation Center
Cameron Station
Alexandria, Virginia 22314

12 cys ATTN: TC

Director
Defense Nuclear Agency
Washington, D. C. 20305

1 cy ATTN: STTL
1 cy ATTN: DDST
3 cys ATTN: RAAE
1 cy ATTN: RAEV

Joint Chiefs of Staff
Department of Defense
Washington, D. C. 20301

1 cy ATTN: J-6

Director
National Security Agency
Fort George G. Meade, Maryland 20755

2 cys ATTN: Technical Library

Under Secretary of Defense (Research and Engineering)
Department of Defense
Washington, D. C. 20301

2 cys ATTN: DDS&SS

Department of Commerce

U. S. Department of Commerce
Office of Telecommunications
Institute for Telecommunication Sciences
National Telecommunications and Information Administration
Boulder, Colorado 80303

2 cys ATTN: W. F. Utlaut

Department of the Army

Commander/Director
Atmospheric Sciences Laboratory
U. S. Army Electronics Command
White Sands Missile Range, New Mexico 88002

1 cy ATTN: DRSEL-BL-SY-S
F. E. Niles

Director
U. S. Army Ballistic Research Laboratories
Aberdeen Proving Grounds, Maryland 21005

1 cy ATTN: George E. Keller

Commander
U. S. Army Foreign Sciences and Technology Center
220 7th Street, N. E.
Charlottesville, Virginia 22901

1 cy ATTN: Robert Jones

Department of the Navy

Chief of Naval Operations
Department of the Navy
Washington, D. C. 20350

1 cy ATTN: NOP 985
1 cy ATTN: NOP 094H

Cheif of Naval Research
Department of the Navy
800 North Quincy Street
Arlington, Virginia 22217

1 cy ATTN: Code 465, R. G. Joiner
1 cy ATTN: Code 427, H. Mullaney

Commander
Naval Electronic Systems Command
Department of the Navy
Washington, D. C. 20360

1 cy ATTN: PME-117
1 cy ATTN: PME-117T
1 cy ATTN: PME 117-21
1 cy ATTN: PME 117-21A
1 cy ATTN: PME 117-22

Director
Naval Ocean Systems Center
Electromagnetic Propagation Division
271 Catalina Boulevard
San Diego, California 92152

1 cy ATTN: Code 2200, W. F. Moler
1 cy ATTN: Code 2200, Ilan Rothmuller
1 cy ATTN: Code 2200, John Bickel

Director
Naval Research Laboratory
4555 Overlook Avenue, S. W.
Washington, D. C. 20375

1 cy ATTN: Code 7700, Timothy P. Coffey
1 cy ATTN: Code 7709, Wahab Ali
2 cys ATTN: Code 7750, John Davis
1 cy ATTN: Code 2627

Commander
Naval Surface Weapons Center (White Oak)
Silver Spring, Maryland 20910

1 cy ATTN: Technical Library

Office of Naval Research Branch Office (Pasadena)
1030 East Green Street
Pasadena, California 91106

1 cy

Department of the Air Force

Commander
Air Force Geophysical Laboratory, AFSC
L. G. Hanscom Air Force Base, Massachusetts 01731

1 cy ATTN: OPR, James Ulwick
1 cy ATTN: LKB, W. Swider
1 cy ATTN: LKB, K. Champion

Director
Air Force Technical Applications Center
Patrick Air Force Base, Florida 32920

1 cy ATTN: TD
1 cy ATTN: HQ 1035th TCHOG/TFS

Department of Defense Contractors

General Electric Company
TEMPO - Center for Advanced Studies
816 State Street
Santa Barbara, California 93102

1 cy ATTN: Warren S. Knapp
1 cy ATTN: DASIAC

Lockheed Missiles and Space Company
3251 Hanover Street
Palo Alto, California 94304

1 cy ATTN: J. B. Reagan
1 cy ATTN: W. Imhof
1 cy ATTN: Martin Walt

Mission Research Corporation
735 State Street
Santa Barbara, California 93101

1 cy ATTN: M. Scheibe
1 cy ATTN: D. Sowle

Pacific-Sierra Research Corporation
1456 Cloverfield Boulevard
Santa Monica, California 90404

1 cy ATTN: E. C. Field

Pennsylvania State University
Ionospheric Research Laboratory
College of Engineering
318 Electrical Engineering - East Wing
University Park, Pennsylvania 16802

1 cy ATTN: John S. Nisbet
1 cy ATTN: Les Hale
1 cy ATTN: A. J. Ferraro
1 cy ATTN: H. S. Lee

R & D Associates
4640 Admiralty Way
Marina Del Rey, California 90291

1 cy ATTN: R. Lelevier
1 cy ATTN: F. Gilmore
1 cy ATTN: R. Turco

The Rand Corporation
1700 Main Street
Santa Monica, California 90406

1 cy ATTN: Cullen Crain

Professor Chalmers F. Sechrist
155 Electrical Engineering Building
University of Illinois
Urbana, Illinois 61801

1 cy ATTN: C. Sechrist

Stanford Research Institue
333 Ravenswood Avenue
Menlo Park, California 94025

1 cy ATTN: Allen M. Peterson
1 cy ATTN: Ray L. Leadabrand